

## Seasonal and interannual variability of particulate organic carbon within the Southern Ocean from satellite ocean color observations

David B. Allison,<sup>1</sup> Dariusz Stramski,<sup>1</sup> and B. Greg Mitchell<sup>2</sup>

Received 28 February 2009; revised 4 January 2010; accepted 21 January 2010; published 3 June 2010.

[1] We use field data of particulate organic carbon (POC) concentration and spectral remote-sensing reflectance,  $R_{rs}(\lambda)$ , to develop an empirical algorithm for estimating POC from ocean color in the Southern Ocean. The algorithm based on the band ratio  $R_{rs}(443)/R_{rs}(555)$  is used in conjunction with Sea-viewing Wide Field-of-View Sensor satellite data to demonstrate seasonal and interannual variability in POC from 1997 to 2007. The surface POC concentrations generally range from 30 to 120 mg m<sup>-3</sup>. On a whole basin scale (south of 35°S), the monthly means are mostly 70–80 mg m<sup>-3</sup>. The seasonal signal is weakest at lower latitudes within the Sub-Antarctic Zone and most pronounced at higher latitudes (>55°S). The area-integrated stock of water column POC in the upper 100 m shows small interannual variations and no clear evidence for long-term trend during the examined 10 year period. The seasonal maximum of the POC stock occurs in December and reaches a value of about 0.6 Pg of carbon for the entire basin south of 35°S. The seasonal range of area-normalized POC is between about 5.5 and 6.6 g m<sup>-2</sup>. The region south of 55°S provides a dominant contribution to the accumulation of POC within the Southern Ocean during the productive period of the season. During the austral spring, the area-normalized POC accumulates in these high-latitude waters at rates from about 0.2 to 0.7 g m<sup>-2</sup> month<sup>-1</sup>. The comparison of these rates with large-scale satellite-based estimates of net primary production indicates that only a small fraction (<10%) of production accumulates as POC.

**Citation:** Allison, D. B., D. Stramski, and B. G. Mitchell (2010), Seasonal and interannual variability of particulate organic carbon within the Southern Ocean from satellite ocean color observations, *J. Geophys. Res.*, 115, C06002, doi:10.1029/2009JC005347.

### 1. Introduction

[2] The Southern Ocean is a unique oceanic domain that encircles the globe providing a link for exchanges of water masses and climatically significant quantities between the world's major ocean basins and atmosphere. Numerous recent studies have been motivated by a need to advance an understanding of the role of the Southern Ocean in regulating atmospheric CO<sub>2</sub> over time scales relevant to climate change and how the ecosystem structure and biogeochemical cycles of the Southern Ocean respond to climate change [e.g., Sarmiento and Orr, 1991; Sarmiento *et al.*, 2004; Le Quéré *et al.*, 2007]. The Southern Ocean, in particular a region of the Antarctic Circumpolar Current between 40° and 60°S, has been identified as a contemporary net sink for atmospheric CO<sub>2</sub> on an annual basis, but the magnitude of

this sink is not firmly established [e.g., Metzl *et al.*, 1999; Takahashi *et al.*, 2002; McNeil *et al.*, 2007].

[3] The drawdown of atmospheric CO<sub>2</sub> into the ocean is favored by (1) the increase in the CO<sub>2</sub> solubility in the cold high-latitude surface waters that sink to form the deep waters of the ocean and (2) biological uptake of CO<sub>2</sub> via phytoplankton photosynthesis in the euphotic zone of the ocean, which results in the production of particulate and dissolved forms of organic carbon that is then partly exported into the deep sea. The ice-free Southern Ocean is the largest of several oceanic regions with high-nutrient, low-chlorophyll (HNLC) characteristics, where major macronutrients (nitrate, phosphate, silicate) occurring in significant concentrations in surface waters are under utilized by autotrophic processes [Martin *et al.*, 1990; Mitchell *et al.*, 1991; Banse, 1996]. These characteristics indicate that the capacity of the biological pump to export organic carbon out of the euphotic layer within the majority of the Southern Ocean is less than its potential maximum. Recent experimental and modeling studies showed, however, relatively high estimates of efficiency of the biological pump exporting particulate organic carbon (POC) [Honjo *et al.*, 2000; Trull *et al.*, 2001; Schlitzer, 2002]. Potential changes in the efficiency of the

<sup>1</sup>Marine Physical Laboratory, Scripps Institution of Oceanography, University of California, San Diego, La Jolla, California, USA.

<sup>2</sup>Integrative Oceanography Division, Scripps Institution of Oceanography, University of California, San Diego, La Jolla, California, USA.

Southern Ocean's biological pump are of interest because they may affect air-sea CO<sub>2</sub> fluxes and levels of atmospheric CO<sub>2</sub> [e.g., *Knox and McElroy*, 1984; *Sarmiento and Toggweiler*, 1984; *Siegenthaler and Wenk*, 1984].

[4] An assessment of biological controls of the carbon cycle, including the efficiency of the biological pump and air-sea CO<sub>2</sub> fluxes, requires determinations of various carbon reservoirs as well as the processes responsible for transformations and transport of carbon, such as primary production, remineralization, and export of organic carbon. POC in the surface ocean, which consists of autotrophic and heterotrophic plankton and biologically derived detrital particles, is one of the reservoirs of substantial importance. The biological pump that exports organic carbon out of the surface ocean is effected largely by sinking particles, which provides a mechanism for a long-term storage of atmospheric CO<sub>2</sub> in the deep ocean [*Volk and Hoffert*, 1985; *Longhurst and Harrison*, 1989]. In addition, the net change of POC in the surface ocean is a component of net community production (NCP), which is defined as gross primary production minus respiration by all the autotrophic and heterotrophic organisms [e.g., *Eppley*, 1989]. As the NCP describes the net amount of organic carbon produced, it is equivalent to the net amount of inorganic carbon biologically consumed in surface waters. Therefore, the NCP integrated within the euphotic layer over a certain period of time determines the role of biological activities for the inorganic carbon budget in surface waters and can also provide a useful constraint for estimating export production out of the euphotic layer if sufficient information about carbon mass balance components, including the net change of POC, is available [*Bates et al.*, 1998; *Hansell and Carlson*, 1998; *Sweeney et al.*, 2000; *Sabine et al.*, 2004].

[5] The stock of POC in the upper ocean is highly variable and its large-scale distributions and long-term variations are poorly characterized. Historically, the large-scale estimates of this variability have been difficult to derive with confidence, primarily because conventional oceanographic sampling has been both temporally and spatially sparse. Recent efforts to develop remote-sensing algorithms for estimating POC in the upper ocean from satellite imagery of ocean color offer significant potential for extending temporal and spatial scales of observations in marine biogeochemical studies [*Stramski et al.*, 1999; *Loisel et al.*, 2001; *Mishonov et al.*, 2003; *Stramska and Stramski*, 2005; *Gardner et al.*, 2006; *Pabi and Arrigo*, 2006; *Stramski et al.*, 2008; *Son et al.*, 2009]. The commonly accepted empirical approach to develop algorithms for estimating seawater constituent concentrations from the spectral ocean reflectance (ocean color) requires the simultaneous collection of in situ data of relevant optical quantities and seawater constituents. Whereas relatively large amounts of such field data have been collected over the years to allow the development of chlorophyll algorithms [e.g., *O'Reilly et al.*, 1998, 2000], the amount of data relevant for the POC algorithm development is much more limited. Only a few studies exist in which the development of POC algorithms is based on an adequate suite of simultaneously collected in situ data that include POC, ocean reflectance, and inherent optical properties (IOPs) of seawater [*Stramski et al.*, 1999; *Stramska and Stramski*, 2005; *Pabi and Arrigo*, 2006; *Stramski et al.*, 2008]. Clearly, due to the limited availability of adequate field data

and their limited geographic coverage, further work in this direction is required.

[6] In this study we use field data collected on several cruises in the Southern Ocean to develop an empirical algorithm that relates surface concentration of POC to the blue-to-green band ratio of remote-sensing reflectance,  $R_{rs}$ . Our primary objective is to apply the algorithm to satellite data of Sea-viewing Wide Field-of-View Sensor (SeaWiFS) and examine seasonal and interannual variability in POC within the surface waters of the Southern Ocean during a period from September 1997 through December 2007.

## 2. Field Experiments

[7] Optical and POC measurements were made during several oceanographic cruises within three regions of the Southern Ocean spanning a time period from 1997 through 2006. These regions include the waters near Antarctic Peninsula and South Shetland Islands (LMG04, AMLR04, and AMLR06 cruises), the Antarctic Polar Frontal Zone (PFZ) within the Pacific sector (REV98 cruises), and the Ross Sea (NBP97 cruise) (Figure 1). The stations were located in high-latitude waters south of 50°S. Most stations were south of 60°S. During each cruise vertical profiles of optical data were collected from several instruments either mounted on the ship's CTD/rosette system for simultaneous in situ measurements with discrete water sampling or deployed shortly before or after the CTD/rosette cast. These deployments of the CTD/rosette and optical instruments constitute a common station. Data collected at the common station are considered "coincident in time and space" for the purposes of development of the POC algorithm. The measurements of direct interest to this study include in situ vertical profiles of radiometric quantities from which the remote-sensing reflectance was determined and the analysis of water samples for the determinations of POC concentration. We restrict our algorithm development to the use of POC and optical data from open water stations where it is reasonable to assume that optical properties and suspended particles are dominated by plankton microorganisms and plankton-derived organic matter.

### 2.1. In Situ Radiometric Measurements

[8] Underwater vertical profiles of spectral downwelling irradiance,  $E_d(z, \lambda)$ , and upwelling radiance from the nadir direction,  $L_u(z, \lambda)$  (where  $z$  is depth and  $\lambda$  light wavelength in vacuo), were made with several calibrated radiometers (Biospherical Instruments, Inc.), each having a number of wave bands in the visible and ultraviolet spectral regions. Specifically, we used MER-2040 and MER-2048 profiling radiometers that were mounted on an optical package lowered by the ship's winch, or PRR-600 and PRR-800 radiometers deployed as free-falling instruments.

[9] The radiometric measurements and data processing were consistent with methods described in NASA protocols [*Mueller et al.*, 2003]. Profiles were visually inspected for quality, the data were binned into 1 m depth intervals, and the near-surface data (usually the top 3–5 m) were rejected from the analysis to avoid surface wave effects. A depth range within the upper mixed layer (typically 5–20 m) was then selected for extrapolation of  $E_d(z, \lambda)$  and  $L_u(z, \lambda)$  to immediately beneath the sea surface using the vertical

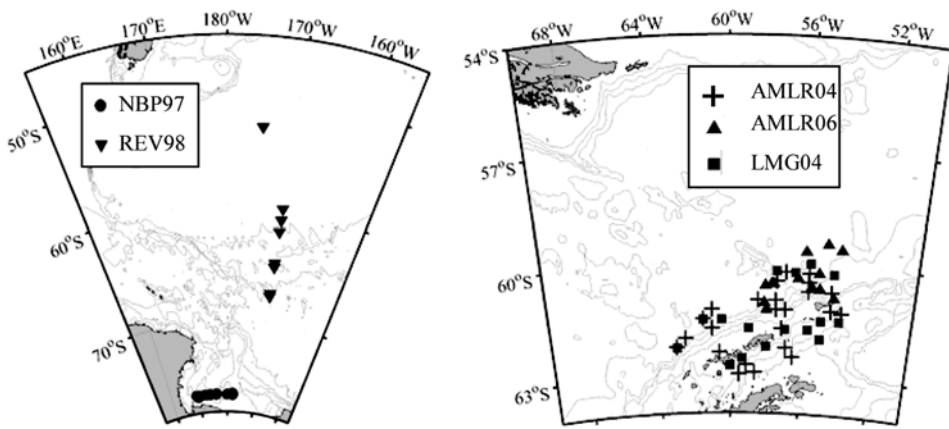


**Figure 1.** Locations of stations in the Southern Ocean where measurements used in the development of POC algorithm were made. The NBP97 stations were visited during the U.S. Joint Global Ocean Flux Study (JGOFS) cruise (NBP9711) in the Ross Sea in November–December of 1997. The REV98 stations represent the JGOFS cruises REV9801 and REV9802 which took place from January through March 1998. The AMLR stations were visited during the January–March period in 2004 and 2006 on the AMLR04 and AMLR06 cruises of the NOAA Fisheries’ U.S. Antarctic Marine Living Resources Program. Additionally, one set of data was collected during the 2004 AMLR season by NSF sponsored cruise LMG0402.

attenuation coefficients for downwelling irradiance ( $K_d$ ) and upwelling radiance ( $K_{Lu}$ ). The estimates of  $E_d(z = 0^-, \lambda)$  and  $L_u(z = 0^-, \lambda)$  just beneath the surface were propagated through the surface to yield the above-water estimates of downward irradiance,  $E_d(z = 0^+, \lambda) \equiv E_s(\lambda)$ , and water-leaving radiance,  $L_u(z = 0^+, \lambda) \equiv L_w(\lambda)$ . The effective coefficients for propagating  $E_d$  and  $L_u$  through the water-air interface were:  $E_d(z = 0^+, \lambda)/E_d(z = 0^-, \lambda) = 1/0.957$  and  $L_u(z = 0^+, \lambda)/L_u(z = 0^-, \lambda) = 0.5425$ . The value of 0.5425 for the transmittance coefficient for  $L_u$  corresponds to the refractive index of water,  $n_w = 1.343$ , which is a reasonable value representative of the visible spectral range [e.g., Mobley, 1994].

[10] In the final step of computations, the spectral remote-sensing reflectance just above the water surface was obtained as  $R_{rs}(\lambda) = L_w(\lambda)/E_s(\lambda)$ . With the values for the effective transmittance coefficients for radiance and irradiance assumed in this study, the relationship between  $R_{rs}(\lambda)$  and its counterpart reflectance just below the surface is:  $R_{rs}(\lambda) = 0.519 L_u(z = 0^-, \lambda)/E_d(z = 0^-, \lambda)$ . For the purposes of POC algorithm development, our interest in this study is focused on the  $R_{rs}(\lambda)$  values from the blue and green spectral regions.

## 2.2. POC Determinations

[11] Discrete water samples were collected from Niskin bottles triggered at several depths within the upper water column extending typically to 200 m during CTD/rosette profiles. For the determinations of POC concentration, suspended particles were collected by filtration under low vacuum of measured volumes of water samples onto pre-combusted (450°C for 4 h) 25 mm Whatman glass fiber filters (GF/F). After filtration, the samples were rinsed with 0.01N HCl to remove inorganic carbon, transferred to sterile glass vials, dried at 55°C in a clean oven, and stored until post cruise analysis in the laboratory. POC was determined by high temperature combustion of sample filters via stan-

dard CHN analysis [Parsons *et al.*, 1984; Knap *et al.*, 1994]. Blank filters were also collected during the cruises to quantify background POC. Precombusted blank GF/F filters were placed on the filtration rig with a small amount of deionized water for the same period of time needed to filter samples of seawater. The blank filters were then processed the same way as sample filters.

[12] The final values of POC concentration were calculated by subtracting the mass of organic carbon on blank filters from the mass of carbon on sample filters, and then dividing this result by the measured volume of filtered sample. For the AMLR04, LMG04, and AMLR06 cruises, replicate POC samples were taken for each depth examined and averaged to produce the final POC concentration; otherwise the POC estimate was obtained from the analysis of a single sample filter. For the development of the POC algorithm we only consider data collected at near-surface depths (<10 m). The POC data between the surface and the depths exceeding 100 m are considered in the development of the relationship between the surface POC and the water column integrated (0–100 m) POC stock.

## 3. Results and Discussion

### 3.1. Reflectance Band Ratio Algorithm for POC

[13] Our approach for developing algorithms to estimate surface POC concentration from ocean reflectance relies on empirical relationships between surface POC and the blue-to-green (BG) band ratio of remote-sensing reflectance,  $R_{rs}(\lambda_B)/R_{rs}(555)$ . The rationale for the POC band ratio algorithm is similar to that used to estimate chlorophyll-a concentration from reflectance band ratio algorithms. Specifically, in the case of POC algorithm, variations in the BG ratio can be viewed as being driven largely by changes in the spectral absorption coefficient of seawater associated with varying concentration of all kinds of POC-containing particles, which include not only pigmented phytoplankton

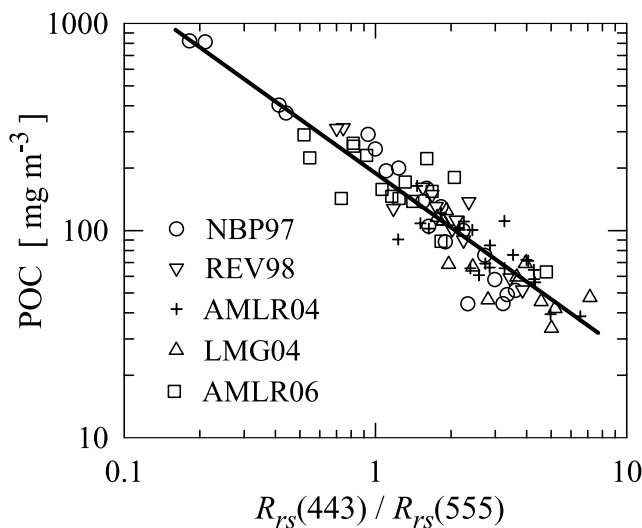


**Figure 2.** Relationship between surface concentration of particulate organic carbon, POC, and the blue-to-green band ratio of remote-sensing reflectance,  $R_{rs}(443)/R_{rs}(555)$ . The data points from several cruises are shown as indicated (the REV98 data are from two cruises REV9801 and REV9802). The power function fit to all data is also shown (solid black line).

but also organic detritus and heterotrophic organisms. All these POC-containing particle types show higher absorption in the blue than in the green spectral region, so their effect on the BG ratio is expected to be qualitatively similar.

[14] We examined the relationship between the surface POC and the following band ratios of reflectance:  $R_{rs}(443)/R_{rs}(555)$ ,  $R_{rs}(490)/R_{rs}(555)$ ,  $R_{rs}(510)/R_{rs}(555)$ , and the maximum band ratio,  $MBR$ .  $MBR$  represents the largest of the three ratios considered.  $R_{rs}(443)/R_{rs}(555)$  was most frequently the largest (55%) and  $R_{rs}(510)/R_{rs}(555)$  was least frequently the largest (15%) among the three ratios considered within our data set. Note that the bands centered at 443, 490, 510, and 555 nm are consistent with the SeaWiFS wave bands [McClain et al., 2004], and these bands are currently used in the NASA algorithm for estimating chlorophyll-*a* concentration in the global ocean [O'Reilly et al., 1998, 2000]. We tested two equations for fitting the data of POC versus reflectance ratio. One equation is the power function and the other equation has the form of the current Ocean Chlorophyll 4 (OC4) algorithm [O'Reilly et al., 2000].

[15] The simple power function of POC versus  $R_{rs}(443)/R_{rs}(555)$  was found to have slightly better error statistics than the other algorithms tested. This power function is  $POC = 189.29 [R_{rs}(443)/R_{rs}(555)]^{-0.870}$ , which is shown in Figure 2 along with the data points. Presently this algorithm appears to be the best choice for the applications in the Southern Ocean. For our data set consisting of 85 measurements that were used to derive this algorithm, the mean normalized bias is 3.2%, the normalized root mean square error is 27.3%, and the determination coefficient is 0.933 (see Stramski et al. [2008] for formulas for calculating the error statistics).

[16] The best fit coefficients for the Southern Ocean algorithms show some differences when compared with the previous analysis of POC and reflectance measurements

taken in other oceanic regions [Stramska and Stramski, 2005; Stramski et al., 2008]. For example, the coefficients of the power function  $POC = A [R_{rs}(443)/R_{rs}(555)]^B$  for the data from the tropical and subtropical waters of the eastern South Pacific and eastern Atlantic Oceans examined by Stramski et al. [2008] were  $A = 203.2$  and  $B = -1.034$ . These differences support the notion that some variability in the empirical band ratio algorithms can be expected within the open waters of the global ocean. Naturally, the optically complex coastal environments present even greater research challenges for ocean color algorithms. In this study, we restricted the algorithm development to the use of data from open water stations and we excluded data from near-coastal stations visited on the AMLR cruises due to potentially significant input of terrigenous material. Some data included in our analysis were collected during an intense bloom of *Phaeocystis antarctica* in the Ross Sea where POC was significantly higher than typical open ocean concentrations (see the NBP97 data points for  $POC > 800 \text{ mg m}^{-3}$  in Figure 2).

[17] It is of interest to note that the use of the blue-to-green reflectance band ratios as inputs to POC and chlorophyll-*a* algorithms implies that both estimated variables are forced to always covary. However, because the band ratio algorithms for POC and chlorophyll-*a* are described by different nonlinear functions, the ratio of the two data products will not be constant over the dynamic range of these variables. Nevertheless, further work on approaches that have potential for more effective decoupling of the remote-sensing estimations of POC and chlorophyll-*a* appears to be warranted [Stramski et al., 2008].

### 3.2. Satellite Estimates of POC in the Southern Ocean

[18] To evaluate the spatial, seasonal, and interannual variations of surface POC in the Southern Ocean, we applied our power function algorithm based on the band ratio  $R_{rs}(443)/R_{rs}(555)$  to the SeaWiFS-derived  $R_{rs}(\lambda)$ . For this analysis the Level 3B standard SeaWiFS data products of normalized water-leaving radiance,  $nL_w(\lambda)$ , binned to a  $9 \times 9 \text{ km}$  equal area grid within monthly intervals spanning a period of over 10 years from September 1997 through December 2007 were obtained from the NASA Ocean Color Web. These data result from SeaWiFS reprocessing 5.2. Because our POC algorithm requires  $R_{rs}(\lambda)$  as input, the satellite estimates of  $nL_w(\lambda)$  were first converted to  $R_{rs}(\lambda)$  using the relationship  $R_{rs}(\lambda) = nL_w(\lambda)/F_o(\lambda)$ , where  $F_o(\lambda)$  is the extraterrestrial solar constant. The values of  $F_o(\lambda)$  were taken from Thuillier et al. [2003]. After determining the satellite estimates of  $R_{rs}(\lambda)$ , the POC algorithm was applied to produce the monthly composites of POC distribution within the Southern Ocean.

#### 3.2.1. Surface Concentration of POC

[19] Maps of monthly mean POC concentrations obtained by averaging data for each month over a 10 year period are displayed in Figure 3. The valid pixels of ocean color data are determined through standard NASA processing after screening for clouds, sun glint, ice cover, atmospheric correction failure, and other failure conditions (e.g., negative  $R_{rs}$ ). The white areas in the maps reflect data that are flagged as invalid with this standard processing. Because of multi-year averaging of monthly composites, significant seasonal change in the white area seen in Figure 3 can be attributed

primarily to winter darkness, short day length, low solar elevation, and seasonal variation in sea ice extent at high latitudes. Other factors, such as cloud cover, appear to have smaller contribution to the extent of data gaps in these multiyear average maps. During the austral autumn, winter, and early spring, large amounts of invalid (flagged) satellite data limit our investigation of POC to lower latitudes, generally north of 50°–55°S. The POC maps for July and August have no valid data south of 55°S. The spatial pattern and seasonal change of white areas in Figure 3 for August through April resemble monthly images of sea ice coverage obtained from passive microwave remote sensing [Comiso *et al.*, 1993; Parkinson, 2004]. For May–July the white areas are also largely related to NASA-flagged invalid ocean color data due to large solar zenith angle.

[20] One of the most striking features of the POC distributions displayed in Figure 3 occurs at latitudes of about 35–40°S within the Subtropical Frontal Zone, STFZ. This zone separates the nitrate replete Sub-Antarctic waters of the Southern Ocean from the lower latitude nitrate-deplete subtropical gyres where primary production is very low [Belkin and Gordon, 1996]. A significant north-to-south increase in POC is observed throughout the year within STFZ all around the globe.

[21] The monthly distributions of POC show significant spatial variability within the Southern Ocean. Elevated POC concentrations generally occur within and downstream of coastal and shelf areas, in regions of major fronts, and areas associated with sea ice retreat. These areas of elevated POC are generally consistent with previous satellite-based estimates of enhanced chlorophyll-*a* concentrations and primary production in the Southern Ocean [Comiso *et al.*, 1993; Sullivan *et al.*, 1993; Arrigo *et al.*, 1998, 2008; Moore and Abbott, 2000]. For example, among the coastal and shelf regions, high POC values often exceeding 150 mg m<sup>-3</sup>, are seen off the east coast of South America, in waters surrounding and downstream of Kerguelen Islands (~50°S, 70°E), off southern Australia and New Zealand, and in some shelf and coastal areas around the Antarctic continent. High POC values are observed in parts of the Ross Sea from December through the rest of austral summer, which can be attributed to the development of phytoplankton blooms in areas of sea ice retreat [Arrigo and McClain, 1994; Arrigo and van Dijken, 2003].

[22] Bands of elevated POC associated with fronts are also apparent in the Atlantic and Indian sectors of the Southern Ocean. These bands occur within two major frontal zones, the Subtropical Frontal Zone, STFZ, and the Polar Frontal Zone, PFZ. Moving from low to high latitudes, the STFZ is bounded by the North Subtropical Front, NSTF, and the South Subtropical Front, SSTF, and the PFZ is bounded by Sub-Antarctic Front, SAF, and the Polar Front,

PF [Belkin and Gordon, 1996]. These frontal structures encompass the flow of the Antarctic Circumpolar Current, ACC. The major oceanic regime north of PFZ is generally regarded as the Sub-Antarctic Zone (SAZ). The regime from the PF southward to the continental margins of Antarctica is the Antarctic Zone (AZ) [Orsi *et al.*, 1995; McNeil *et al.*, 2007]. The AZ encompasses Antarctic surface water masses which are widely subject to winter ice and the effects of melting within the marginal ice zone.

[23] By showing the multiyear monthly means of POC based on averaging data from a 10 year period, Figure 3 highlights the persistent POC features that occur consistently every year or nearly every year in the same areas of the Southern Ocean. The spatial distribution of POC in any given month can, however, vary considerably from year to year. Example illustration of this variability is provided in Figure 4, which compares a 10 year mean distribution of POC for the month of January with the distributions for January 1999, 2001, and 2006. One can see, for example, that the region of very low POC in the southeastern Pacific sector and extending through the southern part of the Drake Passage is significantly more pronounced in January 1999 compared with other images. Another example is the presence of relatively large area of elevated POC within the southeastern Atlantic sector in January 2006. This feature has a much less pronounced expression in other images.

[24] The statistical characteristics of seasonal variability in surface POC are presented in Figures 5 and 6. These calculations were made for the entire Southern Ocean, which for the purpose of this study is defined as the area south of 35°S. The latitude of 35°S is close to the mean position of the North Subtropical Front that is often used to mark the northern border of the Southern Ocean [e.g., Belkin and Gordon, 1996; Moore and Abbott, 2000; MacCready and Quay, 2001]. During the months from November through February, which encompass the peak of the growing season for phytoplankton at high latitudes, the probability density functions of POC are generally broader and show higher frequency of occurrence of relatively high POC > 100–150 mg m<sup>-3</sup> compared with the rest of the year (Figure 5).

[25] The mean and mode values of POC obtained from these probability distributions show moderate seasonal variation (Figure 6a). The maximum value of monthly mean POC slightly above 80 mg m<sup>-3</sup> is observed in December. Similarly high values occur in November and January. The minimum monthly mean POC during the austral winter is below 70 mg m<sup>-3</sup>, but it is important to recall that the estimation of winter values exclude large areas south of 50°–55°S due to the lack of valid SeaWiFS data. The standard deviation varies from about 40 to 50 mg m<sup>-3</sup> for the different months. For each month the standard deviation about the mean represents the combined effect associated

**Figure 3.** (a) The multiyear monthly mean values of POC concentration in the surface waters within the Southern Ocean for austral spring–summer months. Each map was obtained by averaging monthly data collected over a 10 year time period as indicated. The POC concentrations were derived by applying our algorithm based on the  $R_{rs}(443)/R_{rs}(555)$  band ratio to the Level 3B standard binned data of SeaWiFS-derived remote-sensing reflectance. For mapping of surface POC concentrations, the data are projected to an equidistant azimuthal projection. Areas in white represent no satellite data due to winter darkness, sea ice cover, persistent cloudiness, atmospheric correction failure, or other algorithm failure conditions (e.g., low solar elevation, negative  $R_{rs}$ ). The latitude gridlines are shown for 35°S, 45°S, 55°S, and 65°S. The meridians 0°–180° and 90°E–90°W are also shown. (b) As in Figure 3a but for the austral autumn–winter months.

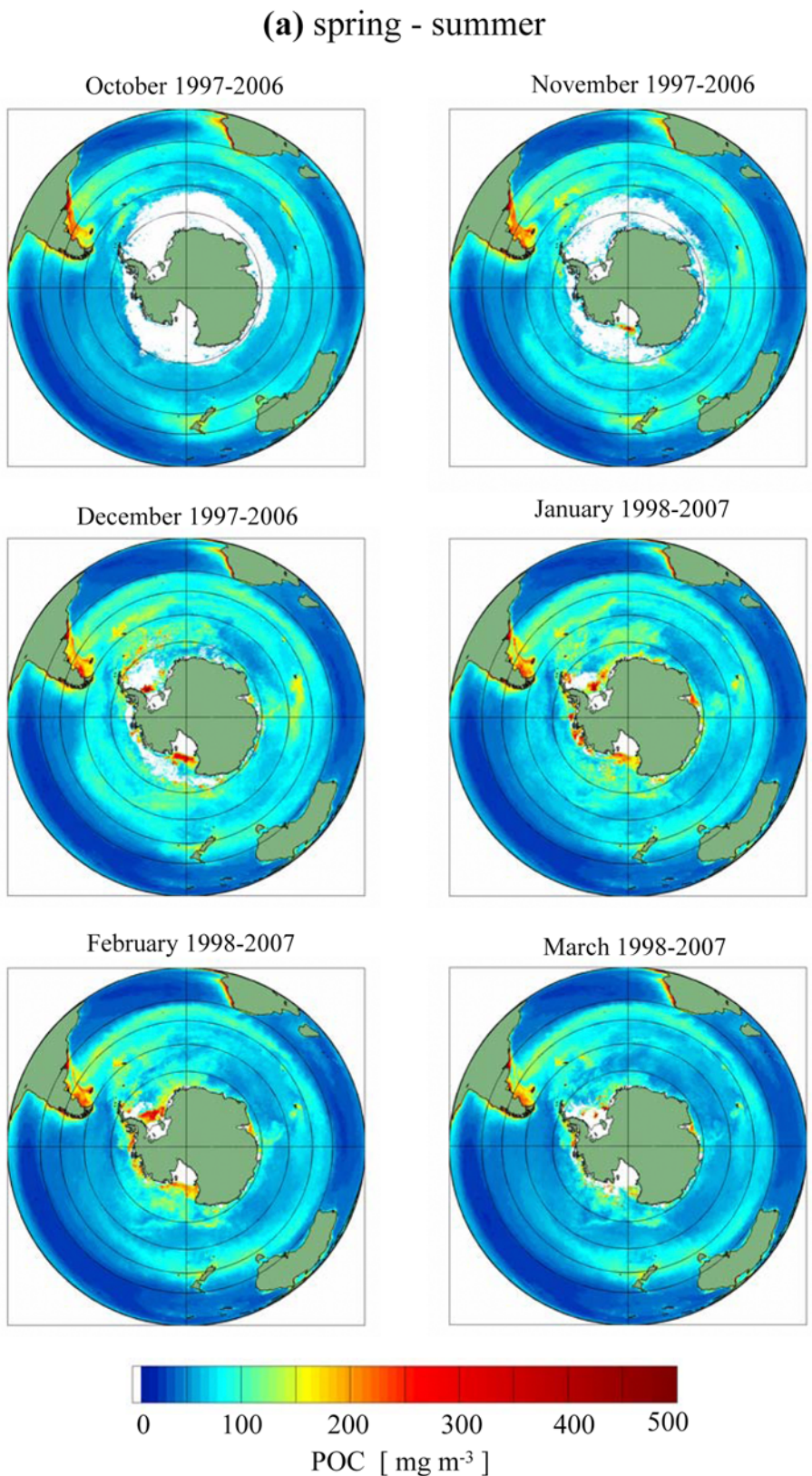


**Figure 3**

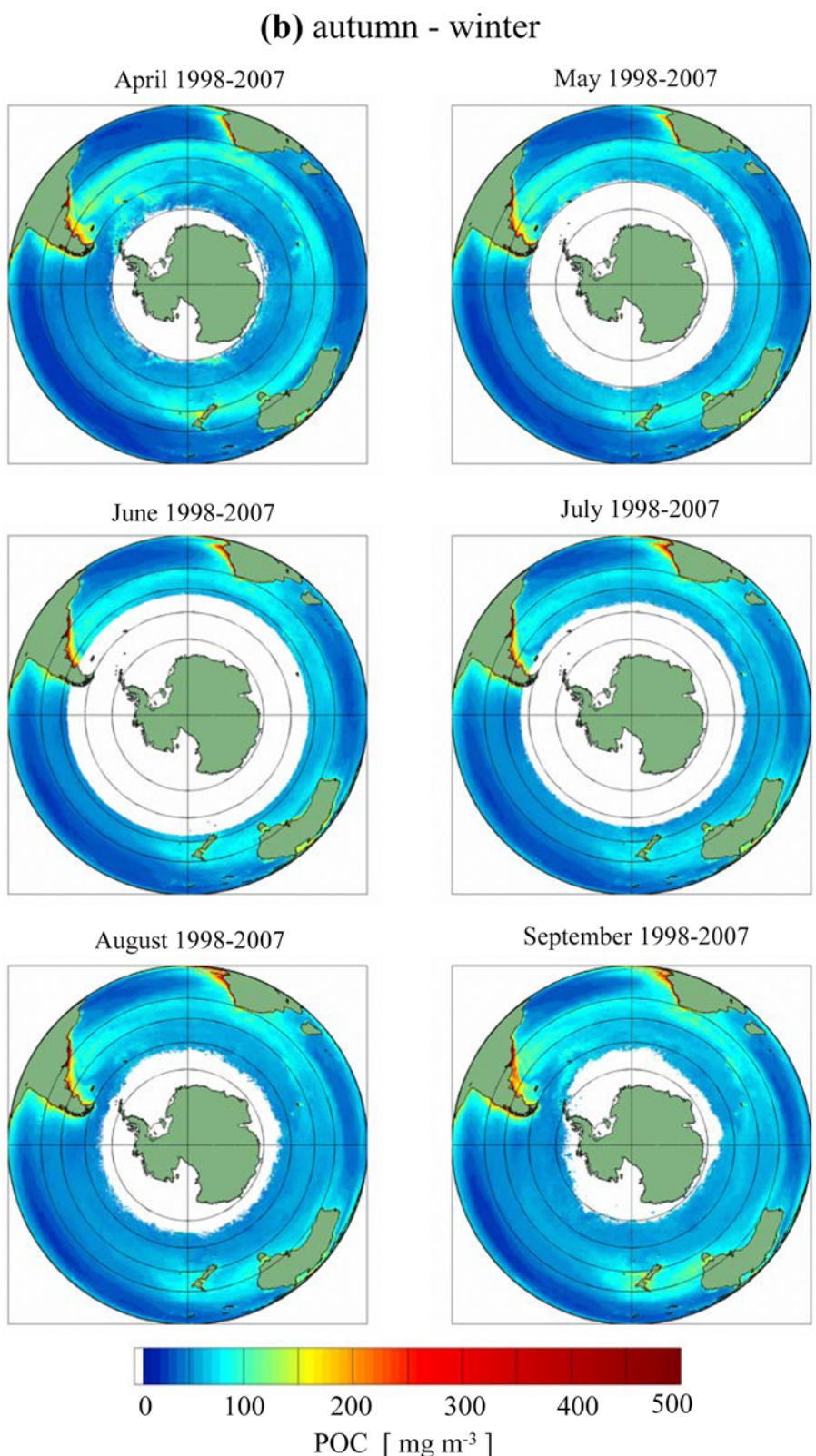


**Figure 3.** (continued)

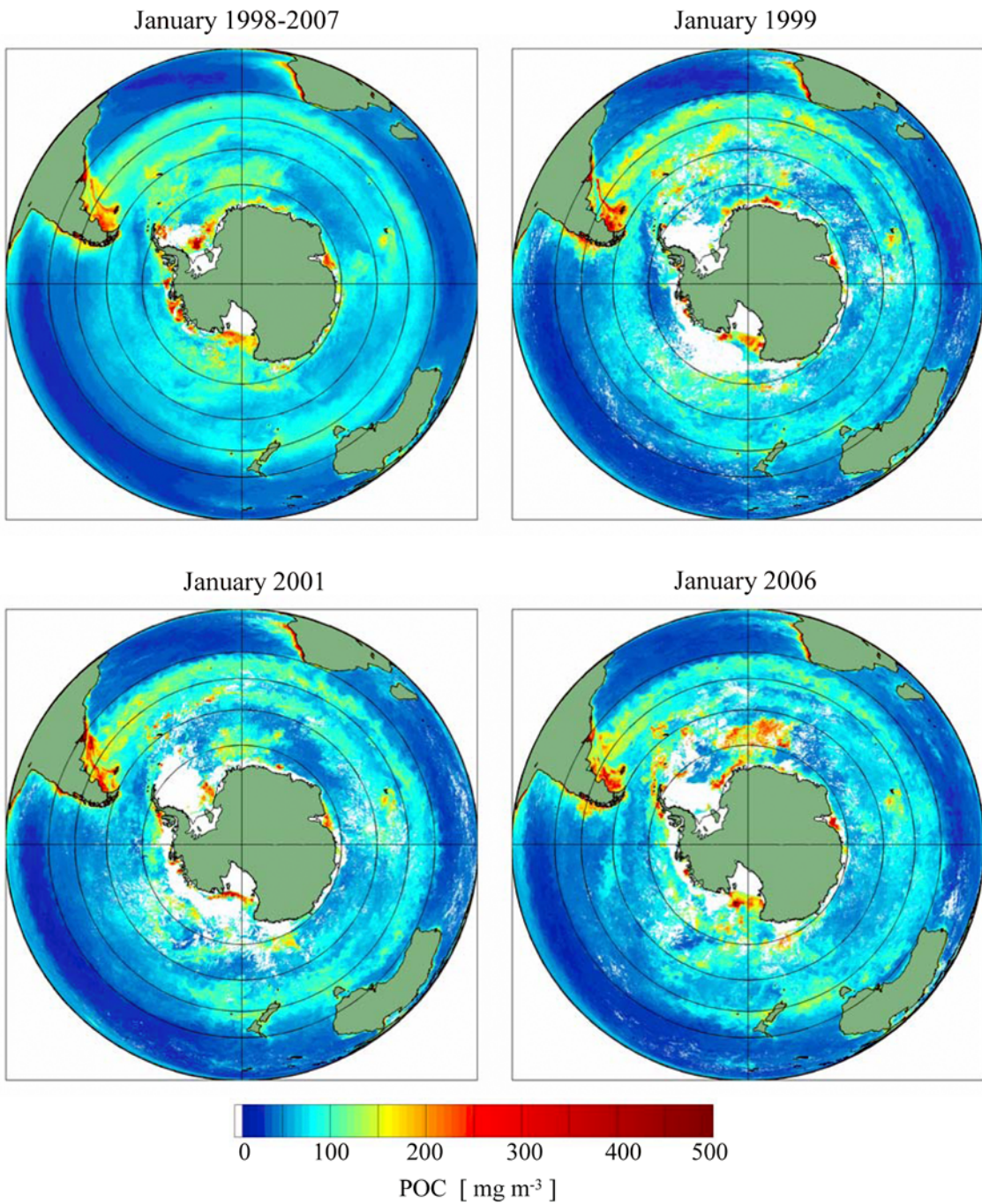


**Figure 4.** Comparison of the monthly mean distribution of POC concentration in the surface waters within the Southern Ocean for the month of January based on averaging data from a time period between January 1998 and January 2007, with the monthly mean distributions for the month of January in three example years: 1999, 2001, and 2006. Areas in white represent no valid satellite data. The latitude grid-lines are shown for 35°S, 45°S, 55°S, and 65°S. The meridians 0°–180° and 90°E–90°W are also shown.

with both the spatial variation of POC within the Southern Ocean and the year-to-year variation. As the probability distributions generally display asymmetry (see Figure 5), the mode is smaller than the mean POC (Figure 6a). For the months of February, March, and April the difference between these statistical parameters is largest, about  $15 \text{ mg m}^{-3}$ .

[26] To illustrate the geographic distribution of POC seasonality, we also calculated zonally averaged POC concentration (Figure 6b). The Southern Ocean shows a significant degree of north-south differentiation by zone in physical, chemical, and biological characteristics [e.g., Deacon, 1982; Pollard *et al.*, 2002]. We defined three latitudinal zones,

$35^{\circ}$ – $45^{\circ}$ S,  $45^{\circ}$ – $55^{\circ}$ S, and south of  $55^{\circ}$ S. As the zones were determined simply by latitude, they can only be roughly related to major oceanic regimes or ecological provinces that are typically defined on the basis of fronts, bathymetry, sea ice coverage, and other physical or biogeochemical features. The  $35^{\circ}$ – $45^{\circ}$ S zone overlaps largely with the Subtropical Frontal Zone, STFZ, and encompasses significant parts of the major oceanic regime of the Sub-Antarctic Zone. This region is also within the ecological province that was referred to as the Sub-Antarctic Water Ring (SWR) in the satellite-based study of chlorophyll distributions and primary production in the Southern Ocean [Moore and Abbott, 2000]. The latitude band between  $45^{\circ}$ S and  $55^{\circ}$ S also largely coincides with the SAZ and the SWR province, especially in the Pacific sector where the mean path of the Antarctic Polar Front (PF) is located south of  $55^{\circ}$ S [Gille, 1994; Orsi et al., 1995; Belkin and Gordon, 1996; Moore

et al., 1999]. Over much of the Atlantic sector and also within the Indian Ocean sector (approximately between  $50^{\circ}$ W and  $150^{\circ}$ E), the mean path for the PF is, however, generally north of  $55^{\circ}$ S and can extend as far north as  $50^{\circ}$ S. In these areas the  $45^{\circ}$ – $55^{\circ}$ S band includes the Polar Frontal Zone.

[27] The large expanses around the Antarctic continent within the latitudinal zone south of  $55^{\circ}$ S also comprise more than just one major oceanic domain or ecological province. As a result of a large latitudinal range in the position of the PF of more than  $10^{\circ}$  (due to steering by continents, islands and bathymetry), the areas south of  $55^{\circ}$ S generally include both the PFZ and AZ in the Pacific sector, and the AZ in the Atlantic and Indian Ocean sectors. At these high latitudes, several distinct ecological regions can be defined on the basis of the variability in the extent of the sea ice cover, bathymetry, and proximity to land, such as the Permanently Open Ocean Zone (POOZ), the Seasonal Ice Zone (SIZ) that contains the Marginal Ice Zone (MIZ), and the coastal and continental shelf zone [Tréquer and Jacques, 1992; Arrigo et al., 1998, 2008; Moore and Abbott, 2000].

[28] Figure 6b compares the seasonal progression of zonally averaged POC concentration. Weakest seasonality is observed in the  $35^{\circ}$ – $45^{\circ}$ S zone where the highest monthly mean POC of about  $80 \text{ mg m}^{-3}$  occurs in October–November and the lowest POC of about  $70 \text{ mg m}^{-3}$  in February–March and then again from June through September. This seasonal variation is somewhat weaker than that calculated for the entire Southern Ocean south of  $35^{\circ}$ S. Our results for low latitudes within the Southern Ocean are consistent with earlier analysis of weak seasonality of phytoplankton pigment concentration in sub-Antarctic waters [e.g., Banse, 1996]. In the  $45^{\circ}$ – $55^{\circ}$ S band, the seasonal signal of POC is stronger, varying between the maximum of about  $90 \text{ mg m}^{-3}$  in December and a minimum of  $60 \text{ mg m}^{-3}$  in August. At higher latitudes south of  $55^{\circ}$ S, the seasonality is even more pronounced. Whereas the maximum mean POC in December is relatively high ( $\sim 87 \text{ mg m}^{-3}$ ), the winter minimum drops to values close to  $50 \text{ mg m}^{-3}$ . We emphasize, however, that no satellite ocean color data are available

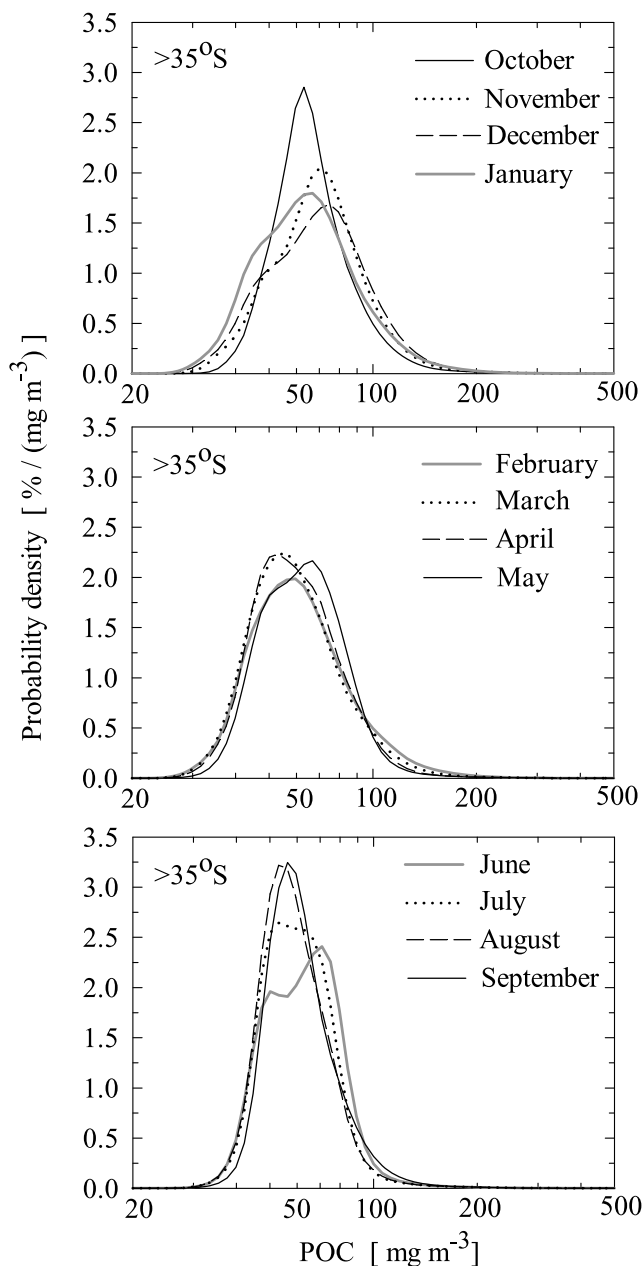


**Figure 5.** The probability density functions of the surface POC concentration within the Southern Ocean (south of  $35^{\circ}$ S) for each month based on the month-by-month analysis of SeaWiFS data over a 10 year period from October 1997 through September 2007. These distributions were created using bins of constant width (0.025) for the log-transformed POC. For a given month (e.g., January), the number of occurrences of POC values within every bin was counted and summed up for all 10 years (i.e., January 1998, January 1999, January 2000, ..., January 2007). To determine the final value of the probability density at a midpoint of a given bin, the ratio of the total count within the bin to the overall total count summed up over all bins was multiplied by 100 and divided by the bin width. In these calculations, the bin width represents the difference in POC between the two end points of the bin expressed as ordinary values of POC (i.e., not logarithmically transformed). For example, for a bin whose midpoint is  $\text{POC} = 10 \text{ mg m}^{-3}$  the bin width is about  $0.576 \text{ mg m}^{-3}$ , and for the midpoint of  $\text{POC} = 100 \text{ mg m}^{-3}$  the bin width is about  $5.76 \text{ mg m}^{-3}$ .

in the months of May, June, and July south of 55°S, which prevents the estimation of winter values.

[29] Figure 6c shows the monthly mean ratio of ocean area with valid ocean color data to the total ocean area for the entire Southern Ocean and the three latitudinal regions considered. These values are calculated relative to the total ocean area within a given region including the areas permanently covered by ice. During winter, the satellite data coverage is limited not only within the region south of 55°S but also to a significant extent within the 45°–55°S latitudinal zone. Only the northernmost zone between 35°S and

45°S exhibits consistently high monthly mean percentage (~96–98%) of valid ocean color pixels throughout the year.

### 3.2.2. Upper Water Column Stock of POC

[30] Our field data show that the surface POC concentration is reasonably well correlated with the mass of POC integrated within the upper water column between the sea surface and a depth of 100 m (Figure 7). At each station the POC determinations were usually made at 4–6 discrete depths from near surface to 150 m. These data were used to obtain the relationship in Figure 7. The limit of 100 m was chosen because our in situ measurements of spectral downwelling irradiance,  $E_d(z, \lambda)$ , indicated that the 1% level of surface irradiance at 490 nm is, on average, at a depth of about 70 m (standard deviation SD = 30 m, number of observations 65). The light close to the 490 nm wave band is usually most penetrating in open ocean waters. To a first approximation, we assume that the 100 m depth delimits the biologically active layer where most organic carbon production via photosynthesis occurs in the open waters of Southern Ocean. The top 100 m layer was used in previous biogeochemical studies of the Southern Ocean, in which the upper water column primary production, net community production, POC stock, and POC export were examined [Gardner et al., 2000; Buesseler et al., 2001; Sweeney et al., 2000; Arrigo et al., 2008].

[31] Using the relationship from Figure 7 and satellite-derived monthly maps of surface POC concentration, we calculated the area-integrated water column standing stock of POC within the upper 100 m of the Southern Ocean. Because at any given time SeaWiFS data are not available for the entire area of the Southern Ocean, it is important to describe in detail the method that we use to calculate the area-integrated stock of POC. For these calculations the Southern Ocean south of 35°S was first divided into 1° circum polar latitudinal bands. Each of these bands was further divided into sectors that have a 10° longitudinal extent. For each sector of 1° (in latitude) × 10° (in longitude) and for each month, we calculated a representative value of monthly mean area-normalized water column integrated POC, denoted as  $\overline{\text{POC}}_{\text{area,sector}}$  [in units of  $\text{g m}^{-2}$ ]. This value of  $\overline{\text{POC}}_{\text{area,sector}}$  was obtained by converting the monthly mean surface concentration of POC [ $\text{mg m}^{-3}$ ] to water column integrated POC [ $\text{g m}^{-2}$ ] (using the relationship from Figure 7) for each pixel within the sector where the SeaWiFS data are available, and then averaging the results for all these valid pixels within each sector. Next, the area-integrated value of water column POC within the sector,

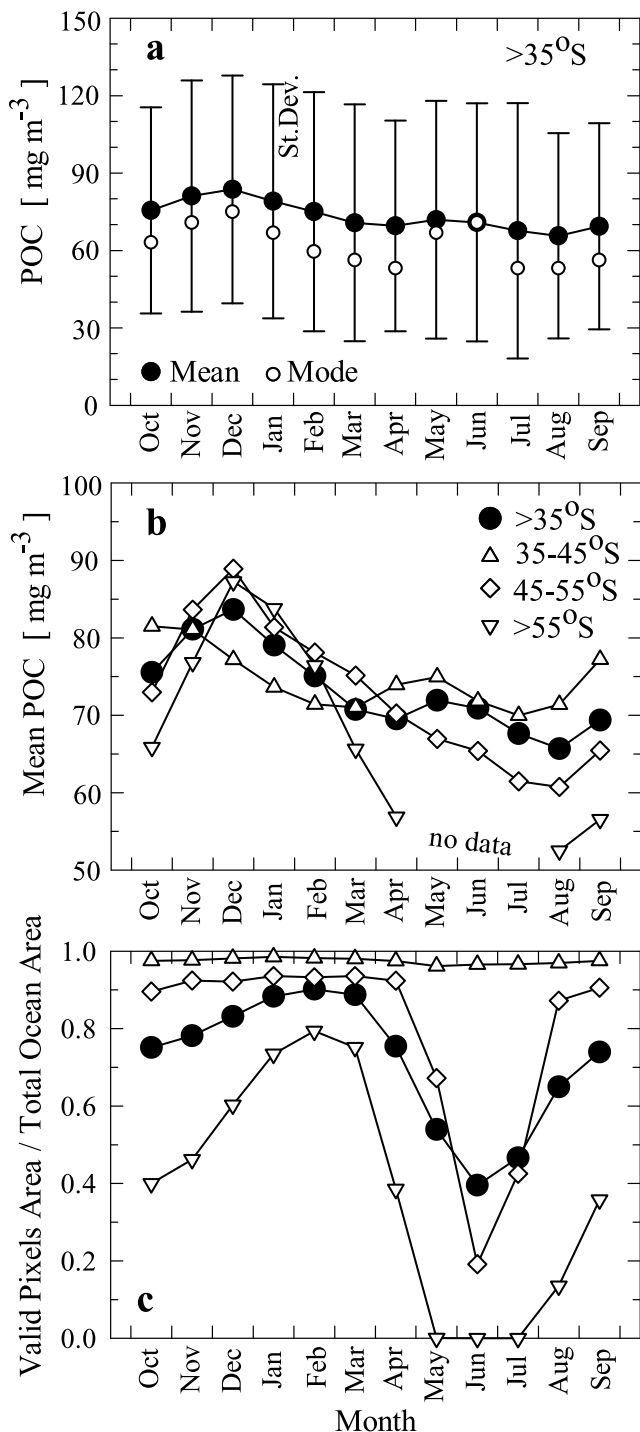


**Figure 6.** (a) Seasonal progression of monthly mean (solid circles) and mode values of surface POC concentration within the entire Southern Ocean (south of 35°S) corresponding to the probability density functions presented in Figure 5. The standard deviation is also shown. (b) Comparison of the monthly mean POC concentration from Figure 6a with similar monthly means for the three latitudinal zones: 35°–45°S, 45°–55°S, and south of 55°S. (c) Monthly mean values of the ratio of ocean area with valid ocean color data pixels to the total ocean area for the entire Southern Ocean and the three latitude bands (see symbols in Figure 6b) based on the month-by-month analysis of SeaWiFS data over a 10 year period from October 1997 through September 2007.

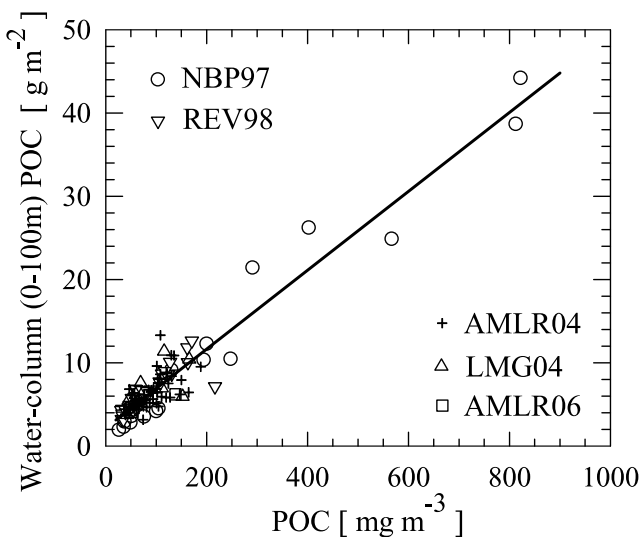


**Figure 7.** The relationship between the water column POC integrated from the sea surface to 100 m depth and the surface concentration of POC obtained from data collected on several cruises in the Southern Ocean as indicated. The best fit linear equation is:  $\text{POC} (\text{water column integrated in } \text{g m}^{-2}) = 0.04737 (\pm 0.00141) \times \text{POC} (\text{surface concentration in } \text{mg m}^{-3}) + 2.16672 (\pm 0.22816)$ . The standard errors of the estimates of the regression coefficients are given in parentheses, the squared correlation coefficient is 0.91, and the number of observations is 115.

$\text{POC}_{\text{int},\text{sector}}$  [ $\text{Pg} = 10^{15}$  g], was determined as a product of  $\overline{\text{POC}}_{\text{area},\text{sector}}$  and the entire ocean area of the sector,  $A_{\text{sector}}$  [ $\text{m}^2$ ]. We note that this method of calculations essentially allows filling of “sporadic” gaps in SeaWiFS data within a given sector (for example, due to clouds, sea ice, sun glint, etc.), and therefore to account for the entire area of the sector, provided that there are some valid pixels within the sector. In this method we assume that the data from the valid pixels provide an average value of  $\overline{\text{POC}}_{\text{area},\text{sector}}$ , which is representative for the entire sector. Hence, the size of each sector is reasonably limited in spatial extent, i.e.,  $1^\circ$  (in latitude)  $\times 10^\circ$  (in longitude). In summary, our method of calculating the area-integrated POC includes the ocean area that is somewhat larger than the area of valid pixels themselves, and excludes the ocean area that is permanently (during a given month) inaccessible to ocean color observations, such as high latitude waters due to winter darkness, ice cover, and large solar zenith angle. In short, in our method a relatively small area “box” (sector) is first chosen ( $1^\circ \times 10^\circ$ ), the average value based on valid pixels within that box is calculated, and then this average value is assigned to all invalid pixels within the box.

[32] In the final step of calculations, the total area-integrated standing stock of POC within the top 100 m water column was estimated by summing up all values of  $\text{POC}_{\text{int},\text{sector}}$  corresponding to all sectors within a region of interest. As in the analysis above, these regions include the entire Southern Ocean south of  $35^\circ\text{S}$  and the three zones, i.e., the  $35^\circ$ – $45^\circ\text{S}$  zone, the  $45^\circ$ – $55^\circ\text{S}$  zone, and the high-latitude region south of  $55^\circ\text{S}$ . The final results of monthly means of area-integrated water column POC for these four major regions are denoted

as  $\text{POC}_{\text{int},>35}$ ,  $\text{POC}_{\text{int},35\text{--}45}$ ,  $\text{POC}_{\text{int},45\text{--}55}$ , and  $\text{POC}_{\text{int},>55}$  [in units of Pg of carbon], respectively.

[33] In the calculations of  $\text{POC}_{\text{int},>35}$ ,  $\text{POC}_{\text{int},35\text{--}45}$ ,  $\text{POC}_{\text{int},45\text{--}55}$ , and  $\text{POC}_{\text{int},>55}$ , we also tested alternative algorithms using sectors with higher resolution in longitude than  $10^\circ$ , specifically  $2^\circ$  and  $5^\circ$ . As expected, the estimates of area-integrated POC stocks decreased somewhat with a decrease in the size of the sector because using larger sectors increased the probability of valid pixels that were then used to represent the entire sector. For example, for the entire Southern Ocean, the  $\text{POC}_{\text{int},>35}$  stocks from the calculations using the highest resolution, i.e., the  $1^\circ$  (in latitude)  $\times 2^\circ$  (in longitude) sectors, were lower on average by about 1.9% than the results from our standard calculations with the  $1^\circ \times 10^\circ$  sectors. In this paper we report the results from the calculations based on the  $1^\circ \times 10^\circ$  sectors.

[34] Because the estimates of area-integrated POC stock depend on the ocean area that is applied in the calculation of these estimates, it is important to show the portion of ocean area, referred to as “applied” ocean area,  $A_{\text{appl}}$ , which contributes to these final estimates of area-integrated POC. Figure 8 shows the monthly mean values of  $A_{\text{appl}}$  as a fraction of the total ocean area. These values are based on averaging data from a 10 year period from October 1997 through September 2007. The year-to-year variations for any given month were small, less than a few percent. As expected, the applied ocean area is generally higher than the ocean area actually associated with valid ocean color pixels shown in Figure 6c because of the “filling” of the full sector if some valid pixels are observed for that sector. For the  $35^\circ$ – $45^\circ\text{S}$  latitudinal zone, the applied area  $A_{\text{appl},35\text{--}45}$  always equals to the total ocean area, i.e., every sector within this zone has always valid pixels with SeaWiFS data (this is not explicitly displayed in Figure 8). In the  $45^\circ$ – $55^\circ\text{S}$  region, the applied area  $A_{\text{appl},45\text{--}55}$  shows a drastic decrease in June–July com-

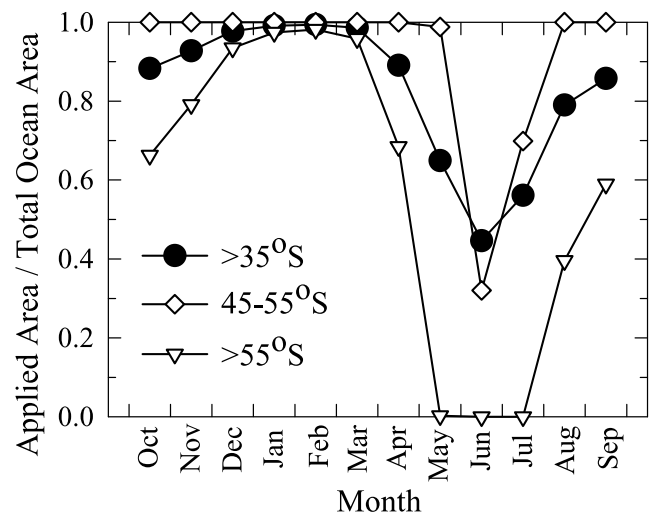


**Figure 8.** Monthly mean values of the ratio of the applied area to the total ocean area within the entire Southern Ocean ( $>35^\circ\text{S}$ ) and the two major regions ( $45^\circ$ – $55^\circ\text{S}$  and south of  $55^\circ\text{S}$ ) based on averaging over a 10 year period from October 1997 through September 2007. The data for the latitude band  $35^\circ$ – $45^\circ\text{S}$  are not displayed because the values in that region are always 1.

**Table 1.** Monthly Mean Values of the Area-Integrated Stock of POC Within the Top 100 m of the Ocean Derived From Satellite Observations of Ocean Color<sup>a</sup>

Month	Southern Ocean >35°S	Southern Ocean 35–45°S	Southern Ocean 45–55°S	Southern Ocean >55°S
January	0.591 (1.3%)	0.195 (2.2%)	0.181 (3.5%)	0.215 (3.1%)
February	0.571 (1.6%)	0.192 (2.2%)	0.176 (3.0%)	0.203 (2.3%)
March	0.553 (1.2%)	0.191 (1.8%)	0.172 (2.0%)	0.190 (1.5%)
April	0.530 (1.2%)	0.196 (1.4%)	0.165 (2.3%)	0.169 (2.0%)
May	0.544 (1.7%)	0.197 (1.4%)	0.158 (2.8%)	no data
June	0.543 (2.3%)	0.192 (1.9%)	0.157 (4.2%)	no data
July	0.525 (2.0%)	0.189 (1.7%)	0.152 (3.0%)	no data
August	0.505 (1.3%)	0.191 (1.5%)	0.151 (1.1%)	0.163 (2.0%)
September	0.528 (1.2%)	0.201 (1.4%)	0.157 (1.2%)	0.170 (2.1%)
October	0.561 (1.1%)	0.208 (1.4%)	0.168 (0.9%)	0.185 (1.9%)
November	0.588 (1.0%)	0.207 (2.3%)	0.182 (2.9%)	0.199 (2.1%)
December	0.607 (1.1%)	0.201 (2.4%)	0.189 (1.7%)	0.217 (2.0%)

<sup>a</sup>The monthly mean is given in units of Pg of carbon. These results were calculated by averaging data from a 10 year period from October 1997 to September 2007. The percent values in parenthesis represent the coefficient of variation due to interannual variability. The results are shown for the entire basin of the Southern Ocean and the three regions within the Southern Ocean. The presented values of the area-integrated stock of POC correspond to the entire ocean area within each region, and were calculated by scaling up the calculations based on the so-called “applied” ocean area (see text for details of the methods).

pared with the rest of the year. There is a strong seasonal variation in the applied area in the region south of 55°S,  $A_{\text{appl},>55}$ , from zero in May–July to over 90% in December–March. As a result, the applied area for the entire Southern Ocean,  $A_{\text{appl},>35}$ , also shows a seasonal variation, with  $A_{\text{appl},>35}$  reduced to less than 50% of the total ocean area in June. We note that the total ocean area for the entire Southern Ocean south of 35°S is about  $9.26 \times 10^{13} \text{ m}^2$ . The total ocean area for the latitude zone 35°–45°S is  $3.23 \times 10^{13} \text{ m}^2$ , for the latitude zone 45°–55°S is  $2.80 \times 10^{13} \text{ m}^2$ , and for the high-latitude region south of 55°S is  $3.23 \times 10^{13} \text{ m}^2$ .

[35] The large seasonal changes in the applied ocean area at high latitudes shown in Figure 8 contribute to the estimation of area-integrated POC stock. Therefore, in addition to calculating the area-integrated stock for the applied ocean area, we also estimated the potential values of the area-integrated POC stock for the entire ocean area in each region considered (Table 1). These latter estimates were obtained by multiplying the applied ocean area-based estimates of POC stock by the ratio of the total ocean area to the applied ocean area. These simple scaling calculations were made for all months and regions considered, with the exception of May, June, and July in the region south of 55°S, where no satellite data are available.

[36] Figure 9 shows the two estimates of the area-integrated stock of POC within the top 100 m of the water column. The results are presented for the monthly mean values based on averaging the data over a 10 year period from October 1997 through September 2007. The interannual variations for any given month were small (the coefficient of variation typically less than 3%) and no evidence of a decadal trend was observed. The seasonal signal in the area-integrated POC is clearly observed, especially during the October–April period for the entire Southern Ocean basin (south of 35°S), the 45–55°S zone, and the southernmost region (>55°S) where this signal is most pronounced. The seasonality of  $\text{POC}_{\text{int},>35}$ ,  $\text{POC}_{\text{int},45–55}$ , and  $\text{POC}_{\text{int},>55}$  is seen in both the estimates based on the applied ocean area and those scaled up to the total ocean area. The seasonal maximum occurs in December. In contrast, the POC stock at lower latitudes within the 35°–45°S zone shows smaller seasonal changes with a maximum earlier in the season during the September–November period.

We recall that in this region, the applied ocean area equals to the total ocean area, so both estimates of  $\text{POC}_{\text{int},35–45}$  are identical.

[37] The differences between the two estimates of area-integrated POC in Figure 9 are obviously largest during the winter months when the applied ocean area represents the smallest fraction of total ocean area. With the exception of the 35–45°S region, the area-integrated POC stocks based on the applied ocean area show a sharp decline during the winter in comparison to the estimates that are scaled up to the total ocean area. Whereas no attempt is made to estimate the winter stocks south of 55°S because of the total lack of data, one can reasonably expect that the true total winter stocks for the entire Southern Ocean will fall between the two estimates displayed in Figure 9. Such expectation also applies to the 45–55°S region. Obtaining winter estimates with higher level of confidence would require the knowledge of POC stocks within large ocean regions covered with ice, which is not available. However, because POC is not zero for ocean water inaccessible by ocean color satellite observations, we expect the total POC stocks to be closer to values scaled to the full ocean area.

[38] The differences between the two estimates of area-integrated POC stocks are smallest during the austral summer maximum (Figure 9). In December, the total area-integrated stock of  $\text{POC}_{\text{int},>35}$  within the Southern Ocean reaches a value of about 0.6 Pg of carbon. It is noteworthy that the three parts of the Southern Ocean defined in our study, the 35°–45°S latitudinal zone, the 45°–55°S zone, and the region south of 55°S, each contribute approximately 0.2 Pg to  $\text{POC}_{\text{int},>35}$  during the summer maximum. We also estimate that the 10 year mean value of  $\text{POC}_{\text{int},>35}$ , as determined over the period from October 1997 through September 2007, is between 0.46 Pg and 0.56 Pg. The lower estimate is based on the calculations for the applied ocean area and the higher estimate is based on the calculations scaled up to the total ocean area.

[39] Because the estimates of area-integrated stock of POC within the upper ocean can be useful for biogeochemical modeling, we provide the monthly mean values of  $\text{POC}_{\text{int},>35}$ ,  $\text{POC}_{\text{int},45–55}$ ,  $\text{POC}_{\text{int},45–55}$ , and  $\text{POC}_{\text{int},>55}$  in Table 1. These estimates are based on scaling our calculations up to the

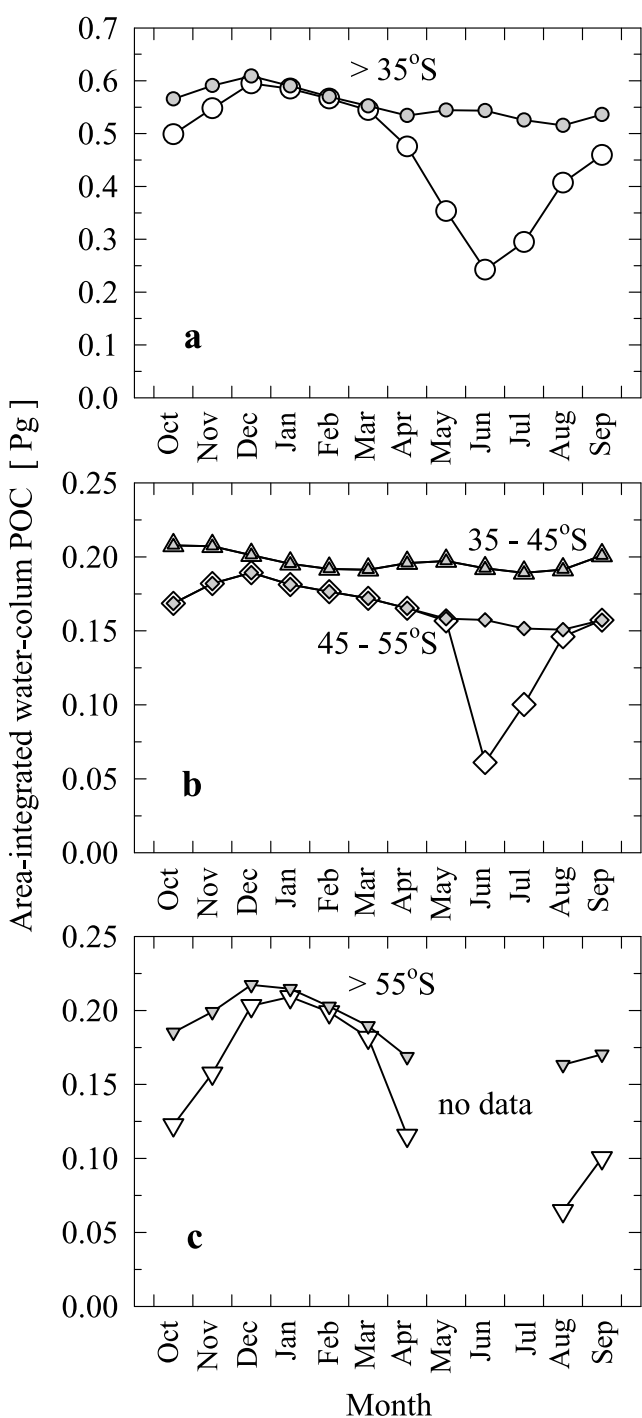


**Figure 9.** Monthly mean values of area-integrated stock of POC within the 100 m upper water column based on averaging over a 10 year period from October 1997 through September 2007 for (a) the entire Southern Ocean ( $>35^{\circ}\text{S}$ ), (b) the  $35^{\circ}$ – $45^{\circ}\text{S}$  and  $45^{\circ}$ – $55^{\circ}\text{S}$  regions, and (c) the region south of  $55^{\circ}\text{S}$ . The open symbols represent the calculations for the applied ocean area. The gray solid symbols represent the calculations scaled up to the total ocean area (see text for details). For the  $35^{\circ}$ – $45^{\circ}\text{S}$  region these two calculations yield identical results. There is no data at latitudes  $>55^{\circ}\text{S}$  for May, June, and July.

total ocean area for each region considered. One may expect that the estimates shown in Table 1 represent the upper bound for the actual POC stocks within the entire ocean areas (including areas with no valid satellite ocean color data). As noted earlier, we expect the true value to be closer to the estimates scaled to total ocean area. Nevertheless, the values presented in Table 1 should be viewed with caution, especially for winter months. Note, for example, that the winter values for the entire Southern Ocean are based on scaling up information acquired at latitudes less than  $55^{\circ}\text{S}$  to the entire ocean area that includes latitudes greater than  $55^{\circ}\text{S}$ .

[40] Although the processes of seasonal accumulation or decline of organic carbon pools in the surface layer of the ocean are now well recognized, the rates of POC changes at large basin and global scales remain uncertain but are required as part of a comprehensive understanding of oceanic mediation of the global carbon cycle. The rate of change of area-integrated POC stock within the 100 m upper water column can be determined by time differencing the satellite-derived data presented in Figure 9. For example, during the October–November–December period the net accumulation of POC within the entire Southern Ocean is  $0.047$ – $0.049\text{ Pg month}^{-1}$  (on the basis of calculations for the applied ocean area) or  $0.018$ – $0.026\text{ Pg month}^{-1}$  (on the basis of scaling to total ocean area). The seasonal accumulation of POC stops in January. The high-latitude waters south of  $55^{\circ}\text{S}$  provide a dominant contribution to the net accumulation of POC within the entire Southern Ocean during the productive season. The average net accumulation of POC south of  $55^{\circ}\text{S}$  during the October–November–December period is  $0.035$ – $0.046\text{ Pg month}^{-1}$  (on the basis of calculations for the applied ocean area) or  $0.014$ – $0.018\text{ Pg month}^{-1}$  (on the basis of scaling to total ocean area).

[41] Figure 10 shows time series of monthly values of area-normalized stocks of POC within the top 100 m layer for the entire Southern Ocean ( $\text{POC}_{\text{area},>35}$ ) and its three regions ( $\text{POC}_{\text{area},35\text{--}45}$ ,  $\text{POC}_{\text{area},45\text{--}55}$ , and  $\text{POC}_{\text{area},>55}$ ) throughout the entire period examined from September 1997 to December 2007. These estimates (in units of  $\text{g m}^{-2}$ ) were obtained respectively as the ratios:  $\text{POC}_{\text{int},>35}/A_{\text{appl},>35}$ ,  $\text{POC}_{\text{int},35\text{--}45}/A_{\text{appl},35\text{--}45}$ ,  $\text{POC}_{\text{int},45\text{--}55}/A_{\text{appl},45\text{--}55}$ , and  $\text{POC}_{\text{int},>55}/A_{\text{appl},>55}$ . In contrast to the area-integrated POC stocks, the area-normalized estimates are virtually insensitive to the size of sectors and the magnitude of applied area used in the calculations. The estimates calculated using different sizes of the sectors agree to within 1% regardless of the month throughout the period of the study.

[42] The seasonal range of  $\text{POC}_{\text{area},>35}$  is between about  $5.5$  and  $6.6\text{ g m}^{-2}$ . This seasonal variation occurs around the multiyear average value of  $6\text{ g m}^{-2}$ . Similar values of the area-normalized POC stock are observed in the three regions although seasonal variability is clearly the largest at latitudes south of  $55^{\circ}\text{S}$ . Within this high-latitude region, the seasonal minimum of  $\text{POC}_{\text{area},>55}$  is about  $5\text{ g m}^{-2}$  and the maximum can reach  $7\text{ g m}^{-2}$ .

[43] Some interannual variations in the area-normalized stocks of POC are also observed. For example, the summer maximum of  $\text{POC}_{\text{area},>35}$  exceeds slightly the value of  $6.6\text{ g m}^{-2}$  in December of 1998, 1999, 2003, 2005, and 2006. In December 2001 and 2007, the  $\text{POC}_{\text{area},>35}$  value is about  $6.4\text{ g m}^{-2}$ .

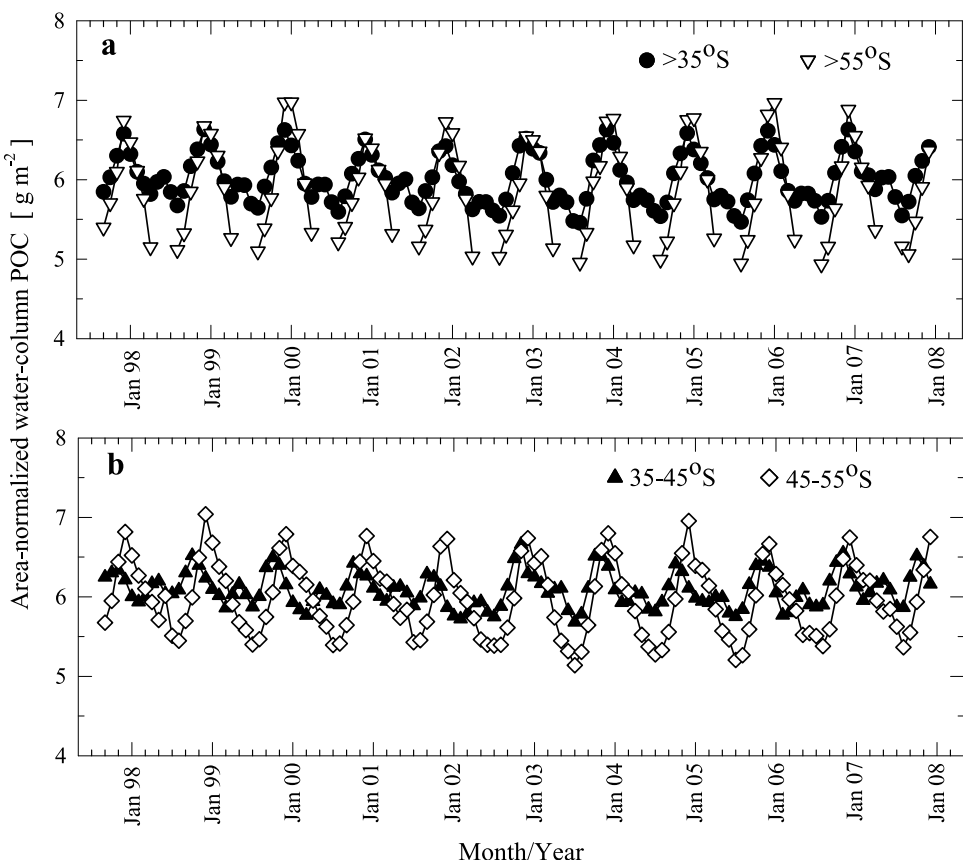


**Figure 10.** Time series of monthly mean values of area-normalized stock of POC within the 100 m upper water column within the entire Southern Ocean ( $>35^{\circ}\text{S}$ ) and the three major regions  $35^{\circ}\text{--}45^{\circ}\text{S}$ ,  $45^{\circ}\text{--}55^{\circ}\text{S}$ , and south of  $55^{\circ}\text{S}$ . There is no data at latitudes  $>55^{\circ}\text{S}$  for May, June, and July.

[44] From Figure 10 one can also estimate net changes in the area-normalized POC stock. Within the entire Southern Ocean, the highest monthly accumulation rates are observed in the period between September and November, when the rates can exceed  $0.3 \text{ g m}^{-2} \text{ month}^{-1}$ . The seasonal accumulation of POC over a period between August and December is on average  $0.99 \text{ g m}^{-2}$  ( $\text{SD} = 0.12 \text{ g m}^{-2}$ ) based on a 10 year data set. For the high-latitude region south of  $55^{\circ}\text{S}$ , the monthly accumulation rates of area-normalized POC stock are, on average,  $0.43 \text{ g m}^{-2} \text{ month}^{-1}$  during September–November period and  $0.56 \text{ g m}^{-2} \text{ month}^{-1}$  in November–December period. The maximum accumulation rate at latitudes  $> 55^{\circ}\text{S}$  occurs between November and December 2006 and exceeds  $0.7 \text{ g m}^{-2} \text{ month}^{-1}$ . The 10 year mean seasonal accumulation of POC for a period from August through December south of  $55^{\circ}\text{S}$  is  $1.64 \text{ g m}^{-2}$  ( $\text{SD} = 0.25 \text{ g m}^{-2}$ ).

### 3.3. Potential Significance of Satellite Observations of POC

[45] Monitoring the rates of change in organic carbon pools in the ocean at large basin scales using satellite-derived data such as those shown in Figures 9 and 10 provides a means for advancing a methodology to diagnose rates and fluxes of relevance to the global carbon cycle and to constrain the uncertainties of carbon budgets. As an example, the satellite-derived net accumulation or decline of

POC in the upper ocean can be used in a carbon mass balance approach to constrain estimates of other components of the carbon budget, including export of organic carbon from the euphotic layer. The uncertainties and scarcity of various data required for rigorous mass balance calculations make this exercise difficult, in particular for large scale calculations within the Southern Ocean. Although such calculations are outside the scope of this paper, we can illustrate this point schematically using a simplified carbon mass balance approach that is based on biological drawdown of dissolved inorganic carbon (DIC) within the euphotic layer.

[46] Because of utilization and production of  $\text{CO}_2$  during photosynthesis and respiration, biologically mediated change in dissolved inorganic carbon ( $\Delta\text{DIC}_{\text{bio}}$ ) is equivalent to net community production, NCP, which is the difference between gross primary production, GPP, and total community respiration, R. The NCP process can result in (1) the net change of POC stock in the euphotic zone,  $\Delta\text{POC}$ ; (2) the net change of DOC (dissolved organic carbon) stock,  $\Delta\text{DOC}$ ; and (3) export of organic carbon,  $\text{POC}_{\text{exp}} + \text{DOC}_{\text{exp}}$ , from the euphotic zone to the deep ocean, largely as sinking biogenic particles (i.e.,  $\text{POC}_{\text{exp}}$ ). Hence, we can write:  $\text{GPP} - \text{R} = \Delta\text{POC} + \Delta\text{DOC} + \text{POC}_{\text{exp}} + \text{DOC}_{\text{exp}}$  or  $\text{NPP} - \text{R}_h = \Delta\text{POC} + \Delta\text{DOC} + \text{POC}_{\text{exp}} + \text{DOC}_{\text{exp}}$ , where NPP is the net primary production and  $\text{R}_h$  the heterotrophic respiration ( $\text{NPP} = \text{GPP} - \text{R}_p$  where  $\text{R}_p$  is phytoplankton respiration). This simplified budget neglects the exchange of organic carbon

laterally via advection and the contribution of calcium carbonate dynamics, and it also assumes that the export term represents the net vertical exchange between the euphotic zone and the underlying layer. The accumulation, decline, and export of POC generally exert strong control on the NCP balance. In particular, during time periods of enhanced seasonal phytoplankton growth, the large impact of biology on the carbon budget is typically associated with accumulation and export of POC.

[47] As an example of such simplified analysis, we can compare our satellite-based estimates of  $\Delta\text{POC}$  obtained from Figure 10 with large-scale satellite-based estimates of NPP in the Southern Ocean during the most productive months. Large-scale estimates of other components of carbon mass balance are generally not available or exhibit significant range, so the pursuit of rigorous closure of mass balance is difficult at this time. There have been several studies utilizing satellite data to estimate distributions of primary production in the Southern Ocean [Arrigo *et al.*, 1998, 2008; Moore and Abbott, 2000]. For example, at the peak of the productive season, the daily rates of NPP within the 100 m upper layer of the pelagic province of the Southern Ocean south of 50°S were estimated to range from 300 to 400 mg C m<sup>-2</sup> day<sup>-1</sup> [Arrigo *et al.*, 2008]. Although regional estimates of production within the marginal ice zone and shelf provinces can be higher, especially during spring phytoplankton blooms, the size of these provinces is much smaller than the pelagic province. Thus, the estimates of area-normalized production for the pelagic province obtained by Arrigo *et al.* [2008] are approximately representative of the entire high-latitude portion of the Southern Ocean, and they can be compared to our POC data for the region south of 55°S. We also note that at the December seasonal peak, other available large-scale estimates of NPP within the high-latitude regions south of the Polar Front (including Permanently Open Ocean Zone, Marginal Ice Zone, and Seasonal Ice Zone) are close to 10 g C m<sup>-2</sup> month<sup>-1</sup> [see Moore and Abbott, 2000, Figure 7]. This result is consistent with the range of daily rates obtained by Arrigo *et al.* [2008].

[48] Compared to the productivity estimates, it is remarkable that the highest seasonal accumulation rates,  $\Delta\text{POC}$ , in the high-latitude region south of 55°S based on our time series of monthly data in Figure 10 are, on average, only about 19 mg C m<sup>-2</sup> day<sup>-1</sup>. These rates are observed in the November–December period. The maximum POC accumulation rates of 24 mg C m<sup>-2</sup> day<sup>-1</sup> were observed in 2006.

[49] An important result from this comparison of  $\Delta\text{POC}$  and NPP is that the POC accumulation rates are less than 10% of net primary production within the high-latitude portion of the Southern Ocean during the most productive part of the season. To support this comparison, we also verified that our area-normalized accumulation rates of POC are nearly the same regardless of whether we use the region south of 55°S or south of 50°S (the latter was used in the study of primary production by Arrigo *et al.* [1998, 2008]). Similar results indicating that  $\Delta\text{POC}$  is a small percentage of NPP, is obtained by comparing our estimates of  $\Delta\text{POC}$  representing the entire Southern Ocean during the most productive period (which are generally less than 12 mg C m<sup>-2</sup> day<sup>-1</sup>) with primary production estimates for oceanic regions south of 35°S [see Moore and Abbott, 2000, Figure 7].

[50] Given that  $\Delta\text{POC}$  is less than 10% of NPP, the major fraction (>90%) of NPP according the mass balance approach must be accounted for by the sum of  $\Delta\text{DOC}$ ,  $\text{POC}_{\text{exp}}$ ,  $\text{DOC}_{\text{exp}}$ , and  $R_h$ . In open ocean regions away from land such as most of the Southern Ocean, a significant portion of the DOC pool is derived from local primary production. As a result, biologically refractory and semi-labile DOC can accumulate in the surface layer where it is then available for export via convective mixing and deep water formation [e.g., Duursma, 1963; Carlson *et al.*, 1994; Hansell *et al.*, 2002]. It has been shown, for example, that during the austral summer in the eutrophic system of the Ross Sea, the fraction of net community production (NCP) accumulating in the upper 150 m as DOC ranges from about 3 to 37% with an average of 14% [Hansell and Carlson, 1998]. During periods of maximum accumulation of total organic carbon in the Ross Sea,  $\Delta\text{POC}$  was shown to account for most of this accumulation, and not  $\Delta\text{DOC}$  [Carlson *et al.*, 2000]. In the context of our comparative analysis of large-scale estimates, one may expect that  $\Delta\text{DOC}$  probably does not exceed 10% of NPP. Therefore, approximately 80% or more of NPP during the most productive months within the upper water column of the Southern Ocean appears to be partitioned as the sum of remineralization ( $R_h$ ) and export ( $\text{POC}_{\text{exp}} + \text{DOC}_{\text{exp}}$ ).

[51] The existing data also suggest that both respiration and export terms can be large or dominant. For example, typical estimates of biological carbon export for open ocean waters of the Southern Ocean during late spring and summer months range between 150 and 300 mg C m<sup>-2</sup> day<sup>-1</sup> [e.g., MacCready and Quay, 2001, and references therein]. The estimates of community respiration,  $R$ , in the mixed layer of the Polar Front region in the Indian Ocean sector during early spring were observed in the range 180–420 mg C m<sup>-2</sup> day<sup>-1</sup> [Aristegui *et al.*, 2002]. Measurements during late spring and summer months in the Pacific sector showed even higher rates of community respiration and suggested a significant contribution of phytoplankton respiration [Dickson and Orchardo, 2001]. These respiration and export data are supportive of our satellite-derived POC in a qualitative sense. Whereas the export and respiration rates represent a large fraction or are comparable to the magnitude of NPP, our data indicate that a small fraction of NPP (<10%) accumulates as POC. As there exists significant physical and biological heterogeneity within the Southern Ocean [e.g., Patterson, 1985; Gille and Kelly, 1996; Longhurst, 1998; Constable *et al.*, 2003], these large-scale estimates of low accumulation of POC during the productive season are, however, not necessarily representative of the Southern Ocean on regional scales. In some Antarctic waters with extremely intense seasonal phytoplankton blooms, for example in the Ross Sea, the POC accumulation can represent a much larger fraction of primary production [Carlson *et al.*, 2000; Gardner *et al.*, 2000].

#### 4. Conclusions

[52] In this study we apply an empirical remote-sensing algorithm for estimating surface POC concentration from ocean color in the Southern Ocean. Using our algorithm based on the blue-to-green reflectance band ratio, we demonstrate variability in POC within the Southern Ocean on

seasonal and interannual time scales during a decade of SeaWiFS satellite mission. Our results show that surface POC concentrations in the Southern Ocean (i.e., at latitudes south of 35°S) generally fall within the range of low to moderate values, from about 30 to 120 mg m<sup>-3</sup>. On a whole basin scale, the monthly means are mostly between 70 to 80 mg m<sup>-3</sup> and the probability of occurrence of POC concentrations above 200 mg m<sup>-3</sup> is very low (Figures 5 and 6a). The seasonal signal in POC is weakest at lower latitudes within the Sub-Antarctic Zone and most pronounced at higher latitudes (>55°S).

[53] Our estimates of the total area-integrated stock of water column POC in the upper 100 m of the Southern Ocean show no clear evidence for a long-term trend in the POC stock during the examined 10 year period from 1997 through 2007. The seasonal variations range from a maximum of 0.6 Pg of carbon in December to a winter minimum, which is uncertain primarily due to incomplete coverage of the ocean area with valid satellite data (Figure 9). We estimate, however, that the winter minimum occurring during the June–August period is within a range of 0.24–0.51 Pg, and probably closer to the upper limit value. During the seasonal maximum (December), the three regions, the 35°–45°S latitudinal band, the 45°–55°S band, and the region south of 55°S, each contribute approximately 0.2 Pg to the total area-integrated stock of POC within the upper 100 m of the Southern Ocean. The seasonal range of area-normalized water column POC for the entire Southern Ocean (>35°S) is between 5.5 and 6.6 g m<sup>-2</sup>, and for the high-latitude region (>55°S) from 5 g m<sup>-2</sup> to 7 g m<sup>-2</sup> (Figure 10). The high-latitude region south of 55°S provides a dominant contribution to the accumulation of POC within the Southern Ocean during the productive period of the season between September and December when the net increase in POC occurs. Then, in these high-latitude waters, the area-normalized POC accumulates at rates between 0.2 and 0.7 g m<sup>-2</sup> month<sup>-1</sup>. The comparison of these rates with large-scale satellite-based estimates of primary production indicates that only a small fraction (<10%) of production accumulates as POC.

[54] Despite limitations of optical remote sensing at high latitudes, especially during winter months, the presented capability to monitor POC from satellite observations will be important to further extend our understanding of the role of POC in ecosystem and carbon dynamics in the Southern Ocean and ecological responses to changing climate. As changing climate and environmental conditions can affect critical carbon fluxes and partitioning of carbon among various reservoirs, the analysis based on satellite observations presented in this study establishes a reference point for potential future change in the pool of particulate organic carbon in the Southern Ocean. Also, because the change in POC stock is one of the components of net community production that describes the carbon mass balance associated with biological processes in the surface ocean, the time series satellite observations of POC can advance an understanding of key questions of the biologically mediated carbon cycle, such as whether oceanic biota act as sources or sinks of carbon and the capacity of the oceanic biological pump to draw down increased levels of atmospheric CO<sub>2</sub>.

[55] **Acknowledgments.** This work was funded by NASA Ocean Biology and Biogeochemistry Program (grant NNG04GO02G awarded to D.S.), NSF Chemical Oceanography Program (OCE-0324680 to D.S.), NASA (G2004-2983 to B.G.M), NSF (ANT0444134 to B.G.M), NASA and NSF (NAG5-7100 and OPP 98-023836 to D.S. and B.G.M.) as part of the U.S. JGOFS Antarctic Environment Southern Ocean Process Study, NSF Graduate Student Fellowship (awarded to D.B.A.), the NOAA Fisheries' U.S. Antarctic Marine Living Resources (AMLR) Program, and the NASA SIMBIOS program. We are grateful to Rick Reynolds, Mati Kahru, Haili Wang, and John Wieland for their invaluable contributions to the execution of our field program and data processing. We also thank the SeaWiFS Project and the NASA's Goddard Earth Sciences Data and Information Services Center DAAC (NASA's Ocean Color Website) for the production and distribution of ocean color data. The technical staff of Antarctic Support Associates, scientists, officers, and crews of the R/V *Nathaniel B. Palmer*, R/V *Roger Revelle*, R/V *Yuzhmorgeologiya*, and R/V *Laurence M. Gould* are acknowledged for providing logistical support and their help onboard during the field work. The analysis of samples for particulate organic carbon was made at Marine Science Institute Analytical Laboratory, University of California, Santa Barbara. We also thank two anonymous reviewers for valuable comments on the manuscript.

## References

- Aristegui, J., M. Denis, J. Alumnia, and M. F. Montero (2002), Water-column remineralization in the Indian sector of the Southern Ocean during early spring, *Deep Sea Res. Part II*, **49**, 1707–1720, doi:10.1016/S0967-0645(02)00008-5.
- Arrigo, K. R., and C. R. McClain (1994), Spring phytoplankton production in the western Ross Sea, *Science*, **266**, 261–263, doi:10.1126/science.266.5183.261.
- Arrigo, K. R., and G. L. van Dijken (2003), Phytoplankton dynamics within 37 Antarctic coastal polynya systems, *J. Geophys. Res.*, **108**(C8), 3271, doi:10.1029/2002JC001739.
- Arrigo, K. R., D. Worthen, A. Schnell, and M. P. Lizotte (1998), Primary production in Southern Ocean waters, *J. Geophys. Res.*, **103**, 15,587–15,600, doi:10.1029/98JC00930.
- Arrigo, K. R., G. L. van Dijken, and S. Bushinsky (2008), Primary production in the Southern Ocean, 1997–2006, *J. Geophys. Res.*, **113**, C08004, doi:10.1029/2007JC004551.
- Banse, K. (1996), Low seasonality of low concentrations of surface chlorophyll in the Subantarctic water ring: Underwater irradiance, iron or grazing?, *Prog. Oceanogr.*, **37**, 241–291, doi:10.1016/S0079-6611(96)00006-7.
- Bates, N. R., D. A. Hansell, and C. A. Carlson (1998), Distribution of CO<sub>2</sub> species, estimates of net community production, and air-sea CO<sub>2</sub> exchange in the Ross Sea polynya, *J. Geophys. Res.*, **103**, 2883–2896, doi:10.1029/97JC02473.
- Belkin, I. M., and A. L. Gordon (1996), Southern Ocean fronts from the Greenwich meridian to Tasmania, *J. Geophys. Res.*, **101**, 3675–3696, doi:10.1029/95JC02750.
- Buesseler, K. O., L. Ball, J. Andrews, J. K. Cochran, D. J. Hirschberg, M. P. Bacon, A. Fleer, and M. Brzezinski (2001), Upper ocean export of particulate organic carbon and biogenic silica in the Southern Ocean along 170°W, *Deep Sea Res. Part II*, **48**, 4275–4297, doi:10.1016/S0967-0645(01)00089-3.
- Carlson, C. A., H. W. Ducklow, and A. F. Michaels (1994), Annual flux of dissolved organic carbon from the euphotic zone in the northwestern Sargasso Sea, *Nature*, **371**, 405–408, doi:10.1038/371405a0.
- Carlson, C. A., D. A. Hansell, E. T. Peltzer, and W. O. Smith Jr. (2000), Stocks and dynamics of dissolved and particulate organic matter in the southern Ross Sea, *Deep Sea Res. Part II*, **47**, 3201–3225, doi:10.1016/S0967-0645(00)00065-5.
- Comiso, J. C., C. R. McClain, C. W. Sullivan, J. P. Ryan, and C. L. Leonard (1993), Coastal Zone Color Scanner pigment concentrations in the Southern Ocean and relationships to geophysical surface features, *J. Geophys. Res.*, **98**, 2419–2451, doi:10.1029/92JC02505.
- Constable, A. J., S. Nicol, and P. G. Strutton (2003), Southern Ocean productivity in relation to spatial and temporal variation in the physical environment, *J. Geophys. Res.*, **108**(C4), 8079, doi:10.1029/2001JC001270.
- Deacon, G. E. R. (1982), Physical and biological zonation in the Southern Ocean, *Deep Sea Res.*, **29**, 1–15, doi:10.1016/0198-0149(82)90058-9.
- Dickson, M.-L., and J. Orchardo (2001), Oxygen production and respiration in the Antarctic Polar Front region during the austral spring and summer, *Deep Sea Res. Part II*, **48**, 4101–4126, doi:10.1016/S0967-0645(01)00082-0.
- Duursma, E. K. (1963), The production of dissolved organic matter in the sea as related to the primary gross production of organic matter, *Neth. J. Sea Res.*, **2**, 85–94, doi:10.1016/0077-7579(63)90007-3.

- Eppley, R. W. (1989), New production: History, methods, problems, in *Productivity of the Ocean: Present and Past*, edited by W. H. Bergeret et al., pp. 85–97, John Wiley, New York.
- Gardner, W. D., M. J. Richardson, and W. O. Smith Jr. (2000), Seasonal patterns of water column particulate organic carbon and fluxes in the Ross Sea, Antarctica, *Deep Sea Res. Part II*, 47, 3423–3449, doi:10.1016/S0967-0645(00)00074-6.
- Gardner, W. D., A. V. Mishonov, and M. J. Richardson (2006), Global POC concentrations from in-situ and satellite data, *Deep Sea Res. Part II*, 53, 718–740, doi:10.1016/j.dsr.2006.01.029.
- Gille, S. T. (1994), Mean sea surface height of the Antarctic Circumpolar Current from Geosat data: Method and application, *J. Geophys. Res.*, 99, 18,255–18,273, doi:10.1029/94JC01172.
- Gille, S. T., and K. A. Kelly (1996), Scales of spatial and temporal variability in the Southern Ocean, *J. Geophys. Res.*, 101, 8759–8773, doi:10.1029/96JC00203.
- Hansell, D. A., and C. A. Carlson (1998), Net community production of dissolved organic carbon, *Global Biogeochem. Cycles*, 12, 443–453, doi:10.1029/98GB01928.
- Hansell, D. A., C. A. Carlson, and Y. Suzuki (2002), Dissolved organic carbon export with North Pacific Intermediate Water formation, *Global Biogeochem. Cycles*, 16(1), 1007, doi:10.1029/2000GB001361.
- Honjo, S., R. Francois, S. Manganini, J. Dymond, and R. Collier (2000), Particle fluxes to the interior of the Southern Ocean in the western Pacific sector along 170°W, *Deep Sea Res. Part II*, 47, 3521–3548, doi:10.1016/S0967-0645(00)00077-1.
- Knap, A., A. Michaels, A. Close, H. Ducklow, and A. Dickson (Eds.) (1994), Protocols for the Joint Global Ocean Flux Study (JGOFS) core measurements, *Manuals IOC Guides* 29, U. N. Educ. Sci. and Cult. Organ., Paris. (Reprinted as *JGOFS Rep.* 19, 170 pp., 1996.)
- Knox, F., and M. B. McElroy (1984), Changes in atmospheric CO<sub>2</sub>: Influence of the marine biota at high-latitude, *J. Geophys. Res.*, 89, 4629–4637, doi:10.1029/JD089iD03p04629.
- Le Quéré, C., et al. (2007), Saturation of the Southern Ocean CO<sub>2</sub> sink due to recent climate change, *Science*, 316, 1735–1738, doi:10.1126/science.1136188.
- Loisel, H., E. Bosc, D. Stramski, K. Oubelkheir, and P.-Y. Deschamps (2001), Seasonal variability of the backscattering coefficient in the Mediterranean Sea based on satellite SeaWiFS imagery, *Geophys. Res. Lett.*, 28, 4203–4206, doi:10.1029/2001GL013863.
- Longhurst, A. R. (1998), *Ecological Geography of the Sea*, 398 pp., Academic, San Diego, Calif.
- Longhurst, A. R., and W. G. Harrison (1989), The biological pump: Profiles of plankton production and consumption in the upper ocean, *Prog. Oceanogr.*, 22, 47–123, doi:10.1016/0079-6611(89)90010-4.
- MacCready, P., and P. Quay (2001), Biological export flux in the Southern Ocean estimated from a climatological nitrate budget, *Deep Sea Res. Part II*, 48, 4299–4322, doi:10.1016/S0967-0645(01)00090-X.
- Martin, J. H., S. E. Fitzwater, and R. M. Gordon (1990), Iron deficiency limits phytoplankton growth in Antarctic waters, *Global Biogeochem. Cycles*, 4, 5–12, doi:10.1029/GB004i001p00005.
- McClain, C. R., G. C. Feldman, and S. B. Hooker (2004), An overview of the SeaWiFS project and strategies for producing a climate research quality global ocean bio-optical time series, *Deep Sea Res. Part II*, 51, 5–42, doi:10.1016/j.dsr.2003.11.001.
- McNeil, B. I., N. Metzl, R. M. Key, R. J. Matear, and A. Corbiere (2007), An empirical estimate of the Southern Ocean air-sea CO<sub>2</sub> flux, *Global Biogeochem. Cycles*, 21, GB3011, doi:10.1029/2007GB002991.
- Metzl, N., B. Tilbrook, and A. Poisson (1999), The annual fCO<sub>2</sub> cycle and the air-sea CO<sub>2</sub> flux in the sub-Antarctic Ocean, *Tellus Ser. B*, 51, 849–861, doi:10.1034/j.1600-0889.1999.t01-3-00008.x.
- Mishonov, A. V., W. D. Gardner, and M. J. Richardson (2003), Remote sensing and surface POC concentration in the South Atlantic, *Deep Sea Res. Part II*, 50, 2997–3015, doi:10.1016/j.dsr.2003.07.007.
- Mitchell, B. G., E. A. Brody, O. Holm-Hansen, C. McClain, and J. Bishop (1991), Light limitation of phytoplankton biomass and macronutrient utilization in the Southern Ocean, *Limnol. Oceanogr.*, 36, 1662–1677, doi:10.4319/lo.1991.36.8.1662.
- Mobley, C. D. (1994), *Light and Water: Radiative Transfer in Natural Waters*, 592 pp., Academic, San Diego, Calif.
- Moore, J. K., and M. R. Abbott (2000), Phytoplankton chlorophyll distributions and primary production in the Southern Ocean, *J. Geophys. Res.*, 105, 28,709–28,722, doi:10.1029/1999JC000043.
- Moore, J. K., M. R. Abbott, and J. G. Richman (1999), Location and dynamics of the Antarctic Polar Front from satellite sea surface temperature data, *J. Geophys. Res.*, 104, 3059–3073, doi:10.1029/1998JC000032.
- Mueller, J. L., G. S. Fargion, and C. R. McClain (Eds.) (2003), Radiometric measurements and data analysis protocols, *Rep. NASA/TM-2003-*211621/Rev4- Vol.III, 78 pp., NASA Goddard Space Flight Cent., Greenbelt, Md.
- O'Reilly, J. E., S. Maritorena, B. G. Mitchell, D. A. Siegel, K. L. Carder, S. A. Garver, M. Kahru, and C. R. McClain (1998), Ocean color chlorophyll algorithms for SeaWiFS, *J. Geophys. Res.*, 103, 24,937–24,953, doi:10.1029/98JC02160.
- O'Reilly, J. E., et al. (2000), Ocean color chlorophyll a algorithms for SeaWiFS, OC2 and OC4: Version 4, *NASA Tech. Memo. 2000-206892*, NASA Goddard Space Flight Cent., Greenbelt, Md.
- Orsi, A. H., T. Whitworth III, and W. D. Nowlin Jr. (1995), On the meridional extent and fronts of the Antarctic Circumpolar Current, *Deep Sea Res. Part I*, 42, 641–673, doi:10.1016/0967-0637(95)00021-W.
- Pabi, S., and K. R. Arrigo (2006), Satellite estimation of marine particulate carbon in waters dominated by different phytoplankton taxa, *J. Geophys. Res.*, 111, C09003, doi:10.1029/2005JC003137.
- Parkinson, C. L. (2004), Southern Ocean sea ice and its wider linkages: Insights revealed from models and observations, *Antarct. Sci.*, 16, 387–400, doi:10.1017/S0954102004002214.
- Parsons, T. R., Y. Maita, and C. M. Lalli (1984), *A Manual of Chemical and Biological Methods for Seawater Analysis*, 173 pp., Pergamon, Oxford, U. K.
- Patterson, S. L. (1985), Surface circulation and kinetic energy distributions in the Southern Hemisphere oceans from FGGE drifting buoys, *J. Phys. Oceanogr.*, 15, 865884 doi:10.1175/1520-0485(1985)015<0865:SCAKED>2.0.CO;2.
- Pollard, R. T., M. I. Lucas, and J. F. Read (2002), Physical controls on biogeochemical zonation in the Southern Ocean, *Deep Sea Res. Part II*, 49, 3289–3305, doi:10.1016/S0967-0645(02)00084-X.
- Sabine, C. L., R. A. Feely, G. C. Johnson, P. G. Strutton, M. F. Lamb, and K. E. McTaggart (2004), A mixed layer carbon budget for the GasEx-2001 experiment, *J. Geophys. Res.*, 109, C08S05, doi:10.1029/2002JC001747.
- Sarmiento, J. L., and J. C. Orr (1991), Three-dimensional simulations of the impact of Southern Ocean nutrient depletion on atmospheric CO<sub>2</sub> and chemistry, *Limnol. Oceanogr.*, 36, 1928–1950, doi:10.4319/lo.1991.36.8.1928.
- Sarmiento, J. L., and J. R. Toggweiler (1984), A new model for the role of the oceans in determining atmospheric pCO<sub>2</sub>, *Nature*, 308, 621–624, doi:10.1038/308621a0.
- Sarmiento, J. L., et al. (2004), Response of ocean ecosystems to climate warming, *Global Biogeochem. Cycles*, 18, GB3003, doi:10.1029/2003GB002134.
- Schlitzer, R. (2002), Carbon export fluxes in the Southern Ocean: Results from inverse modeling and comparisons with satellite based estimates, *Deep Sea Res. Part II*, 49, 1623–1644, doi:10.1016/S0967-0645(02)00004-8.
- Siegenthaler, U., and T. Wenz (1984), Rapid atmospheric CO<sub>2</sub> variations and ocean circulation, *Nature*, 308, 624–626, doi:10.1038/308624a0.
- Son, Y. B., W. D. Gardner, A. V. Mishonov, and M. J. Richardson (2009), Multispectral remote-sensing algorithms for particulate organic carbon (POC): The Gulf of Mexico, *Remote Sens. Environ.*, 113, 50–61, doi:10.1016/j.rse.2008.08.011.
- Stramska, M., and D. Stramski (2005), Variability of particulate carbon concentration in the north polar Atlantic based on ocean color observations with Sea-viewing Wide Field-of-view Sensor (SeaWiFS), *J. Geophys. Res.*, 110, C10018, doi:10.1029/2004JC002762.
- Stramski, D., R. A. Reynolds, M. Kahru, and B. G. Mitchell (1999), Estimation of particulate organic carbon in the ocean from satellite remote sensing, *Science*, 285, 239–242, doi:10.1126/science.285.5425.239.
- Stramski, D., et al. (2008), Relationships between the surface concentration of particulate organic carbon and optical properties in the eastern South Pacific and eastern Atlantic Oceans, *Biogeosciences*, 5, 171–201.
- Sullivan, C. W., K. R. Arrigo, C. R. McClain, J. C. Comiso, and J. Firestone (1993), Distributions of phytoplankton blooms in the Southern Ocean, *Science*, 262, 1832–1837, doi:10.1126/science.262.5141.1832.
- Sweeney, C., D. A. Hansell, C. A. Carlson, L. A. Codispoti, L. I. Gordon, J. Marra, F. J. Millero, W. O. Smith, and T. Takahashi (2000), Biogeochemical regimes, net community production and carbon export in the Ross Sea, Antarctica, *Deep Sea Res. Part II*, 47, 3369–3394, doi:10.1016/S0967-0645(00)00072-2.
- Takahashi, T., et al. (2002), Global air-sea CO<sub>2</sub> fluxes based on climatological surface ocean pCO<sub>2</sub> and seasonal biological and temperature effects, *Deep Sea Res. Part II*, 49, 1601–1622, doi:10.1016/S0967-0645(02)00003-6.
- Thuillier, G., M. Herse, P. C. Simon, D. Labs, H. Mandel, D. Gillotay, and T. Foujols (2003), The solar spectral irradiance from 200 to 2400 nm as measured by the SOLSPEC spectrometer from the ATLAS 1-2-3 and EURECA missions, *Sol. Phys.*, 214, 1–22, doi:10.1023/A:1024048429145.

- Tréquer, P., and G. Jacques (1992), Dynamics of nutrients and phytoplankton, and fluxes of carbon, nitrogen, and silicon in the Antarctic ocean, *Polar Biol.*, 12, 149–162.
- Trull, T. W., S. G. Bray, S. J. Manganini, S. Honjo, and R. Francois (2001), Moored sediment trap measurements of carbon export in the Subantarctic and Polar Frontal Zones of the Southern Ocean, south of Australia, *J. Geophys. Res.*, 106, 31,489–31,509, doi:10.1029/2000JC000308.
- Volk, T., and M. I. Hoffert (1985), Ocean carbon pumps: Analysis of relative strengths and efficiencies in ocean-driven atmospheric CO<sub>2</sub> changes, in *The Carbon Cycle and Atmospheric CO<sub>2</sub>: Natural Variations*

*Archean to Present, Geophys. Monogr. Ser.*, vol. 32, edited by E. T. Sundquist and W. S. Broecker, pp. 99–110, AGU, Washington, D. C.

---

D. B. Allison and D. Stramski, Marine Physical Laboratory, Scripps Institution of Oceanography, University of California, San Diego, La Jolla, CA 92093-0238, USA. (dstramski@ucsd.edu)

B. G. Mitchell, Integrative Oceanography Division, Scripps Institution of Oceanography, University of California, San Diego, La Jolla, CA 92093-0218, USA.